iScience

CellPress
OPEN ACCESS

Article

The mitochondrial succinate dehydrogenase complex controls the STAT3-IL-10 pathway in inflammatory macrophages

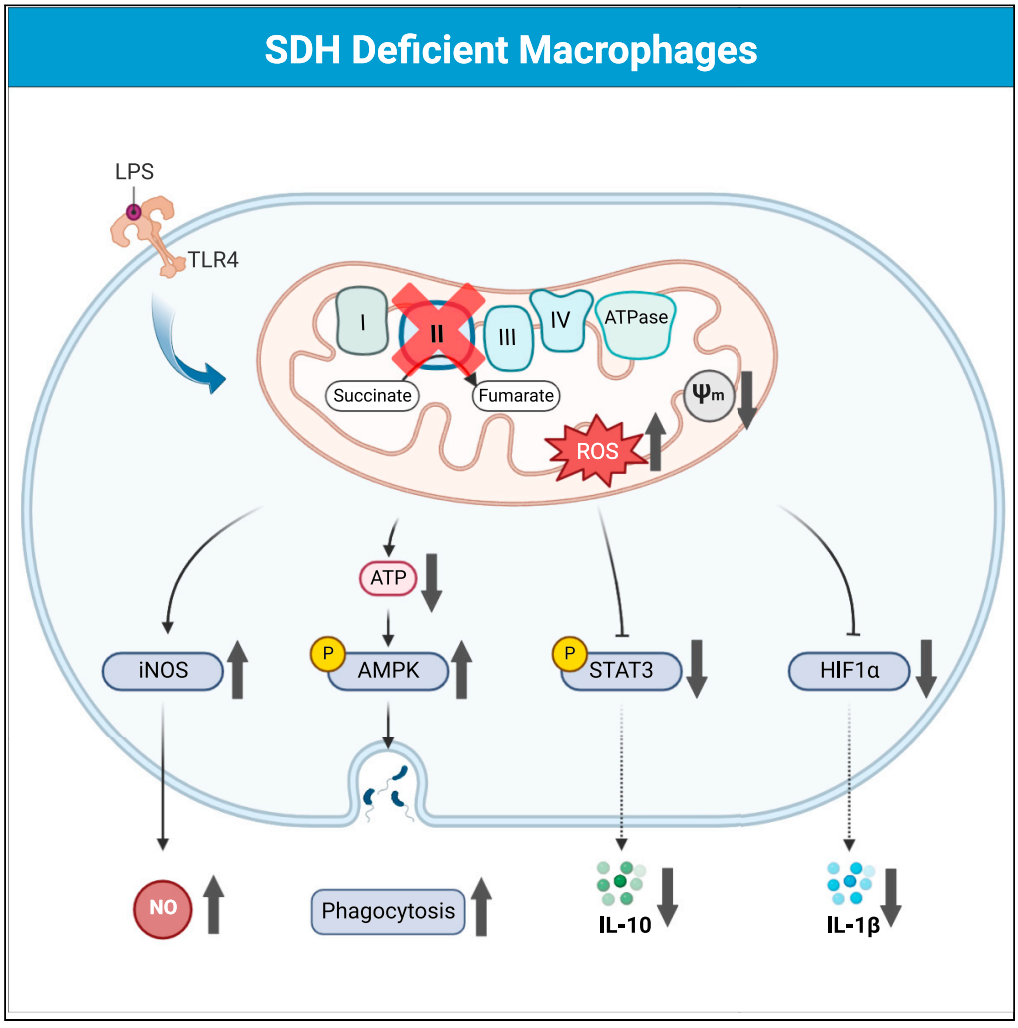

Dino Gobelli, Pablo Serrano-Lorenzo, María J. Esteban-Amo, ..., Miguel Á. Martín-Casanueva, Miguel Á. de la Fuente, María Simarro

msimarrogrande@gmail.com

Highlights

Generation of macrophages deficient in the SDH catalytic subunits Sdha and Sdhb

Both subunits control IL-1β production by LPS-activated macrophages

Both subunits control the STAT3-IL-10 pathway in LPS-activated macrophages

Gobelli et al., iScience 26, 107473
August 18, 2023
https://doi.org/10.1016/j.isci.2023.107473

iScience

CellPress
OPEN ACCESS

Article

The mitochondrial succinate dehydrogenase complex controls the STAT3-IL-10 pathway in inflammatory macrophages

Dino Gobelli,[1,2] Pablo Serrano-Lorenzo,[3,4,5] María J. Esteban-Amo,[1,2] Julia Serna,[2,6] M. Teresa Pérez-García,[2,6] Antonio Orduña,[7,8] Alexis A. Jourdain,[9] Miguel Á. Martín-Casanueva,[3,4,5] Miguel Á. de la Fuente,[1,2,10] and María Simarro[1,2,10,11,*]

SUMMARY

The functions of macrophages are tightly regulated by their metabolic state. However, the role of the mitochondrial electron transport chain (ETC) in macrophage functions remains understudied. Here, we provide evidence that the succinate dehydrogenase (SDH)/complex II (CII) is required for respiration and plays a role in controlling effector responses in macrophages. We find that the absence of the catalytic subunits Sdha and Sdhb in macrophages impairs their ability to effectively stabilize HIF-1α and produce the pro-inflammatory cytokine IL-1β in response to LPS stimulation. We also arrive at the novel result that both subunits are essential for the LPS-driven production of IL-10, a potent negative feedback regulator of the macrophage inflammatory response. This phenomenon is explained by the fact that the absence of Sdha and Sdhb leads to the inhibition of Stat3 tyrosine phosphorylation, caused partially by the excessive accumulation of mitochondrial reactive oxygen species (mitoROS) in the knockout cells.

INTRODUCTION

Mitochondria are responsible for a large variety of physiological processes, including the tricarboxylic acid (TCA) cycle, the electron transfer chain (ETC), and the oxidative phosphorylation (OXPHOS) system for ATP production. Mitochondria also play a central role in both apoptotic and necrotic cell death via the release of apoptogens, cellular Ca2+ homeostasis, oxidative stress, and the biosynthesis of steroid hormones.[1]

Mitochondria are among the most plastic organelles of cells and play an important role in the cellular adaptation to external stimuli. This adaptive role of mitochondria has become very clear in certain immune cells, especially in macrophages, whose functions have been widely reported to be under metabolic control. Macrophages are a heterogeneous population of immune cells playing many diverse functions in immune responses. They are able to change their phenotype and function rapidly and reversibly in response to different environmental signals. Macrophages are classified on a continuum between two extreme phenotypes: a pro-inflammatory (M1) profile and an anti-inflammatory/pro-resolving (M2) profile. M1 macrophages are typically induced by lipopolysaccharide (LPS) and Th1 cytokine interferon gamma (IFN-γ) and they produce pro-inflammatory cytokines, kill pathogens, and initiate adaptive responses. On the other hand, M2 macrophages can be induced by Th2 cytokines, such as interleukin-4 (IL-4), and are characterized by an anti-inflammatory profile, which facilitates the resolution of inflammation and tissue repair.[2] It has been widely reported that the previously mentioned phenotypic and functional changes of macrophages are accompanied by dramatic switches in cell metabolism: while M1 rely mainly on glycolysis for ATP production, M2 macrophages are more dependent on mitochondrial OXPHOS.[3]

Several studies have highlighted the crucial role of metabolic reprogramming in macrophage activation. M1 macrophage activation (e.g., with LPS) leads to a break in the TCA cycle and OXPHOS suppression. One of the hallmarks of M1 macrophage activation is the accumulation of succinate as a result of the break at succinate dehydrogenase (SDH) in the TCA cycle and the production of succinate from glutamine through anaplerosis and the gamma aminobutyric acid shunt pathway.[4,5] A high abundance of succinate induces the stabilization of hypoxia-inducible factor-1α (HIF-1α) as well as the transcriptional activation

[1]Department of Cell Biology, Histology and Pharmacology, Faculty of Medicine, University of Valladolid, 47005 Valladolid, Spain

[2]Unit of Excellence Institute of Biomedicine and Molecular Genetics (IBGM), University of Valladolid and Spanish National Research Council (CSIC), 47003 Valladolid, Spain

[3]Hospital 12 de Octubre Research Institute (imas12), 28041 Madrid, Spain

[4]Biomedical Network Research Centre on Rare Diseases (CIBERER), Instituto de Salud Carlos III, 28029 Madrid, Spain

[5]Mitochondrial Disorders Laboratory, Clinical Biochemistry Department, Hospital Universitario 12 de Octubre, 28041 Madrid, Spain

[6]Department of Biochemistry and Molecular Biology and Physiology, Faculty of Medicine, University of Valladolid, 47005 Valladolid, Spain

[7]Division of Microbiology, Hospital Clínico of Valladolid, 47003 Valladolid, Spain

[8]Department of Microbiology, University of Valladolid, 47005 Valladolid, Spain

[9]Department of Immunobiology, Faculty of Biology and Medicine, University of Lausanne, 1011 Lausanne, Switzerland

[10]These authors contributed equally

[11]Lead contact

*Correspondence: msimarrogrande@gmail.com

https://doi.org/10.1016/j.isci.2023.107473

of the pro-inflammatory cytokine IL-1β in macrophages.[4] Importantly, the oxidation of succinate by SDH is necessary to drive the production of IL-1β.[6] In fact, the inhibition of SDH with dimethyl malonate (DMM) impairs LPS-induced HIF-1α and IL-1β mRNA in macrophages. Accordingly, treatment with DMM efficiently decreased serum levels of IL-1β in a murine model of sepsis induced by LPS.[6] An independent study showed a robust increase in SDH activity in macrophages challenged with *Escherichia coli* or *Salmonella enterica*, supporting that SDH has a role in promoting a pro-inflammatory phenotype.[7] In the same study, mice injected with *E. coli* that were treated with SDH inhibitor nitropropionic acid (3-NPA) showed decreased serum levels of IL-1β.[7] Finally, a very recent study demonstrates that DMM treatment inhibits IL-1β secretion by decreasing NLRP3 inflammasome activation.[8]

SDH, also known as complex II (CII), participates in both the TCA cycle and the ETC and is composed of four subunits (SDHA, SDHB, SDHC, and SDHD).[9] SDHA contains the catalytic binding pocket for succinate and produces FADH2 and fumarate within the TCA cycle. SDHB contains three iron-sulfur clusters that accept the electrons from FADH2 and transfer them to SDHC and SDHD, which are embedded in the inner mitochondrial membrane and constitute the CII function within the ETC serving as the site for ubiquinone binding and reduction to ubiquinol.[9] Previous studies that investigated SDH function in macrophages mainly used DMM and NPA, which are SDHA inhibitors.[6,7] The specific functions of SDHA and the other SDH subunits have been inferred in part from the impact of their mutations on human health. The genetic defects of SDH genes are associated with two very different types of disease. Mutations in SDHA have been linked primarily to severe neurodegenerative diseases including Leigh syndrome and late-onset optic atrophy.[10] However, mutations in subunit SDHB, SDHC, or SDHD are linked to tumorigenesis in the form of familial paragangliomas and pheochromocytomas.[11] The mechanisms underlying these differences are still poorly understood. A study done with different tumor cell lines (Hep3B, A549, and 143B) showed that the inhibition of distal subunits of CII, either pharmacologically or via RNA interference of SDHB, increases mitochondrial reactive oxygen species (mitoROS) production, induces HIF-1α stabilization, and increases cellular growth rates *in vivo* and *in vitro*.[12] However, the inhibition of SDHA, again either pharmacologically or via RNA interference, fails to increase ROS production or induce HIF-1α stabilization and results in decreased growth rates *in vitro* and *in vivo*.[12] More recently, a novel function of SDHA has been identified in a human breast cancer cell line deficient in SDHB. In the absence of SDHB, free SDHA promotes the switch to bioenergetically less-demanding processes and promotes cell growth under nutrient-poor conditions.[13] However, a separate study by Armstrong et al. has shown that *Sdhb* knockout and succinate accumulation are insufficient to initiate tumorigenesis in mouse chromaffin cells, but rather that dual *Sdhb*/*Nf1* loss yields SDHx-like pheochromocytomas.[14] Together, these studies summarized previously highlight that SDHA has a role as a driver of tumorigenesis in SDHB-negative tumors and as a driver in the pro-inflammatory response in macrophages.

This study explores the specific roles of the SDH/CII catalytic subunits, Sdha and Sdhb, in pro- and anti-inflammatory responses in macrophages using state-of-the-art gene deletion methods. In particular, we demonstrate that both Sdha and Sdhb are necessary for proper LPS-mediated IL-1β production and HIF-1α stabilization but are dispensable for IL-6 and tumor necrosis factor alpha (TNF-α) production as previously described using inhibitors. The main novelty of the work lies in the finding that Sdha and Sdhb are essential for IL-10 production and the tyrosine phosphorylation of the transcription factor Stat3.

RESULTS

The absence of Sdha and Sdhb severely impacts mitochondrial respiration in macrophages

To better understand the role played by SDH/CII in macrophage functions (represented in Figure 1A), we generated *Sdha*−/− and *Sdhb*−/− RAW 264.7 murine macrophage cell lines using a CRISPR-Cas9-based strategy, termed homology-independent targeted insertion.[15] As depicted in Figure 1B, we used donor plasmids containing a blasticidin cassette flanked by the same gRNA/Cas9 target sequences located within exon 1 of *Sdha* and *Sdhb*. Following Cas9 cleavage, the blasticidin cassette was integrated via NHEJ. Correctly targeted clones were identified by sequencing (Table S1) and the absence of Sdha and Sdhb proteins was confirmed by Western blotting (Figure 1C). Interestingly, we observed that the absence of Sdha led to the disappearance of Sdhb, while the levels of Sdha remained intact in *Sdhb*−/− cells. This result suggests that unassembled Sdha is more stable than unassembled Sdhb as indicated previously.[13] For its proper enzymatic activity, SDH/CII requires the independent maturation of SDHA, SDHB, and SDHC + SDHD mediated by four subunit-specific chaperones.[9] First, we explored SDH/CII activity in *Sdha*−/− and *Sdhb*−/− macrophage cell lines by measuring the electron transfer from succinate to the

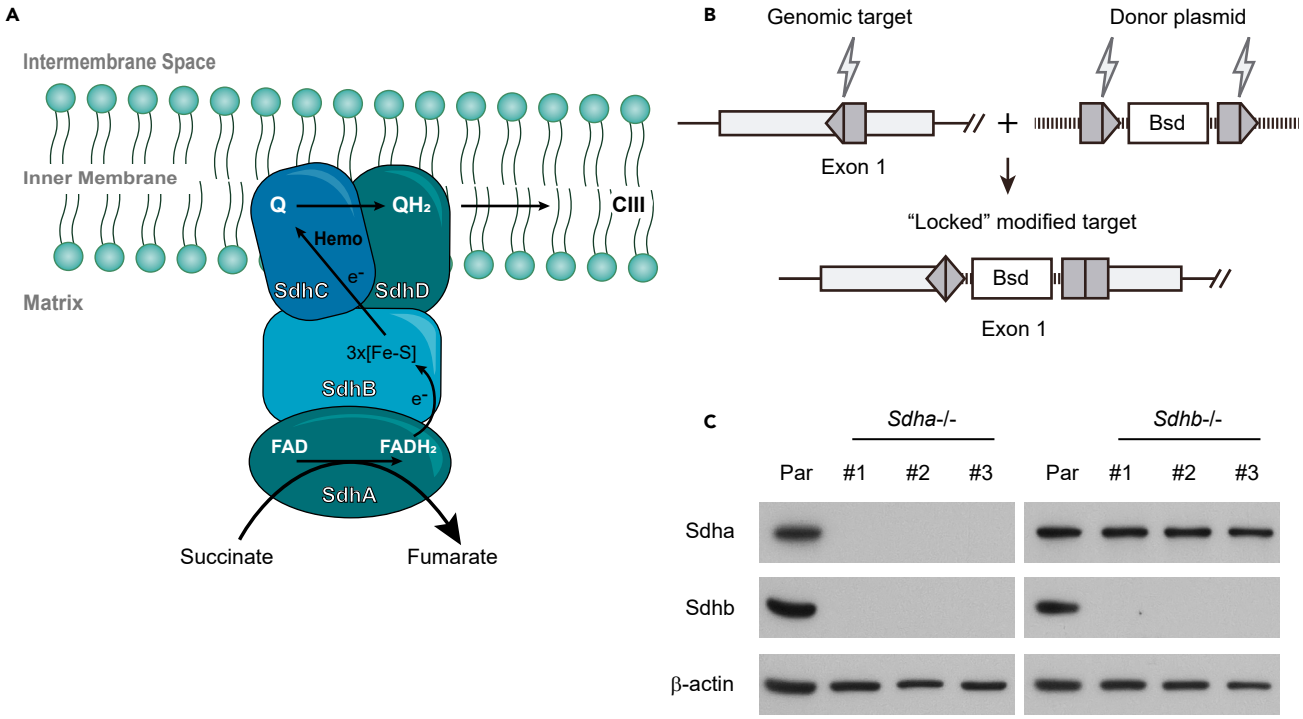

Figure 1. Generation of *Sdha*−/− and *Sdhb*−/− macrophage cell lines

(A) Schematic illustrating the structure and function of SDH/CII. The catalytic subunit SDHA protrudes into the matrix, where it functions to oxidize succinate to fumarate and reduces FAD to FADH2. The electrons released from this reaction are shuttled through the Fe-S clusters through SDHB to reduce the electron carrier ubiquinone (Q) to produce ubiquinol (QH_2) which passes the electrons from complex II to complex III.

(B) General Cas9 HITI strategy to ablate *Sdha* and *Sdhb*. Cas9 produces a double-stranded DNA break at specific target sequences within the first exon of *Sdha* and *Sdhb*. Cas9 also excises the HITI donor by cleaving the same target sequence flanking the blasticidin cassette to be inserted. The excised HITI donor is ligated into the genomic site through the NHEJ pathway. The forward integration depicted in the scheme is "locked" and cannot be processed further. A reverse integration could be corrected by continuous excision/repair cycles in virtue of flanking target sites reconstitution. Gray pentagons represent Cas9/gRNA target sequences. Black lines within pentagons indicate Cas9 cleavage sites.

(C) Whole cell lysates from each resultant knockout cell line were analyzed by Western blotting using antibodies against SDHA, SDHB, or β-actin (loading control). Correctly targeted clones were named *Sdha*−/− or *Sdhb*−/− followed by a serial number Par, parental cell line.

artificial electron acceptor DCPIP via the coenzyme Q10 analog decylubiquinone with an assay that requires an intact complex.[16] As expected, both *Sdha*−/− and *Sdhb*−/− macrophage cell lines lacked SDH/CII activity (Figure 2A). Previous reports have postulated that the accumulation of free SDHA has a role in the pathological phenotypes associated with mutations in *SDHB-D* genes by being involved in off-pathway reactions such as uncoupled succinate oxidation from ubiquinol reduction and ROS formation.[12] Using colorimetric assays, we found that cellular levels of succinate were higher than those in parental cells in both *Sdha*−/− and *Sdhb*−/− macrophage cell lines, whereas levels of fumarate were lower (Figure 2B). These results demonstrate that free Sdha present in *Sdhb*−/− macrophages fails to oxidize succinate, which is in agreement with a previous report that free recombinant human SDHA has inherently low catalytic activity.[17]

Intriguingly, the complete loss of SDHB has been reported to greatly impact basal and maximal respiration capacities and ATP production in different cancer cell types.[13,18] Nevertheless, the impact of the absence of SDHA and SDHB on macrophage respiration remain unexplored. Only one study has documented that the use of the SDHA inhibitor NPA leads to a decrease in spare respiratory capacity.[7] Emerging research on macrophage metabolism has revealed profound changes in metabolic profiles during activation.[2] In this regard, it is well documented that activation of macrophages through the LPS-TLR4 pathway decreases oxygen consumption and ATP/ADP ratio, and increases glycolysis.[6,19,20] Next, we assessed the mitochondrial respiratory profile of *Sdha*−/− and *Sdhb*−/− macrophages untreated or treated with LPS. Oxygen consumption rate (OCR) was measured before and after the sequential addition of oligomycin (ATP synthase inhibitor), the carbonyl cyanide 4-(trifluoromethoxy)phenylhydrazone (H+ ionophore), and rotenone

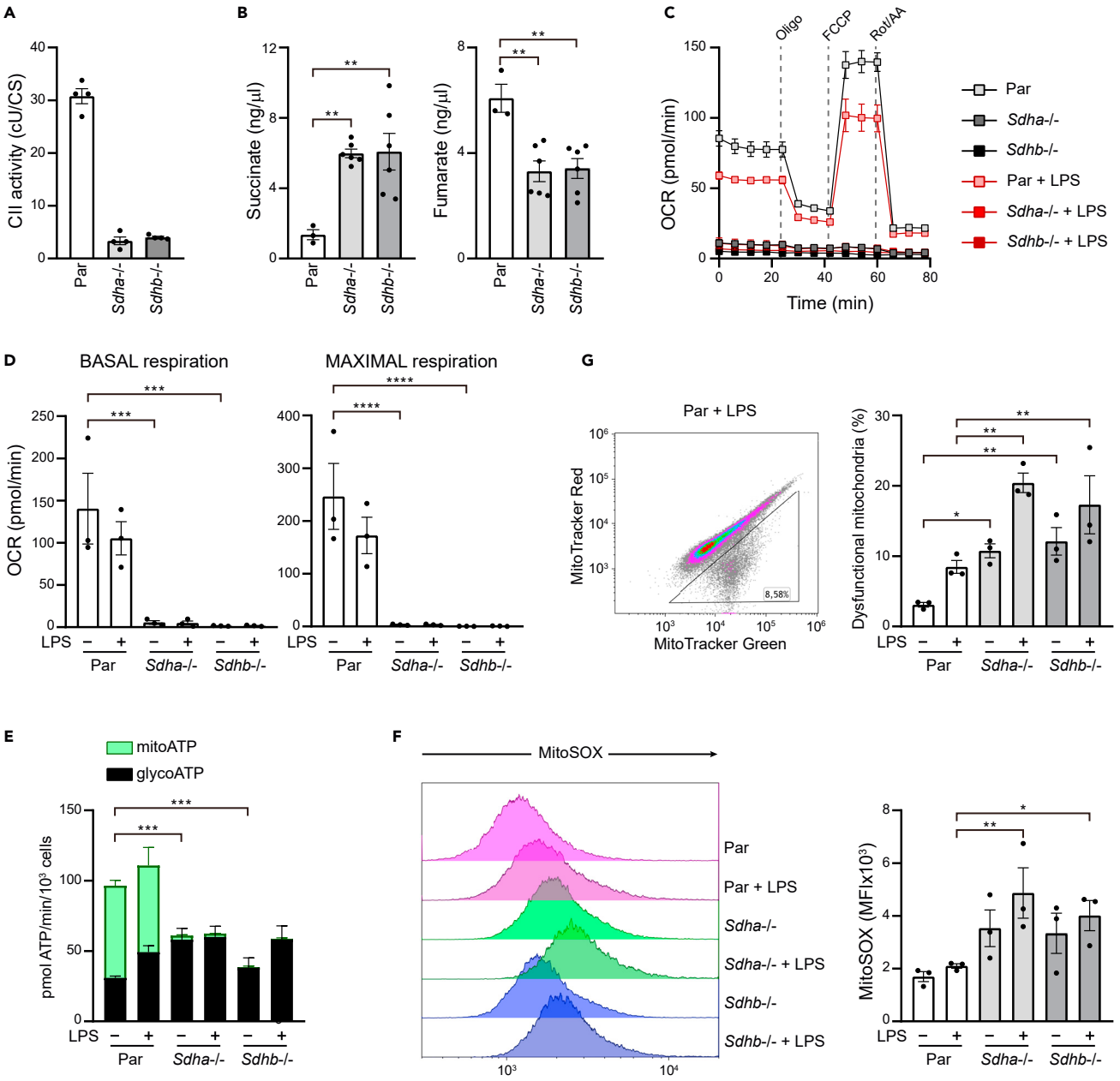

Figure 2. Respiration in *Sdha*−/− and *Sdhb*−/− macrophages

(A) Spectrophotometric activity of complex II, normalized to citrate synthase activity in mitochondria isolated from parental (Par), *Sdha*−/− and *Sdhb*−/− RAW 264.7 cells.

(B) Cellular levels of succinate and fumarate in extracts from the indicated RAW 264.7 sublines.

(C) OCR in RAW 264.7 sublines were measured under basal conditions and after the sequential addition of oligomycin (2.6 µM), FCCP (1 µM), and a combination of rotenone (Rot) and antimycin A (1 µM).

(D) Basal respiration, maximal respiration, and (E) ATP production.

(F) Representative flow cytometry histograms of MitoSOX staining (left) and graph showing relative mitoROS levels (right).

(G) Representative flow cytometry plots (left) showing the gating strategy for the detection of MitoTracker Green^{+high} MitoTracker Red^{+low} cells and graph (right) showing the percentage of dysfunctional mitochondria. When indicated, cells were treated with LPS prior to the assays. *, $p < 0.05$; **, $p < 0.01$; ***, $p < 0.005$; ****, $p < 0.001$. Each point represents a biological replicate. Data are shown as the mean ± SEM.

(CI inhibitor) (Figure 2C). As shown in Figure 2D, basal and maximal respiration capacities were severely impaired in both LPS-treated and untreated *Sdha*−/− and *Sdhb*−/− macrophages. Consistent with these data, total ATP production in *Sdha*−/− and *Sdhb*−/− macrophages relied exclusively on glycolysis and was

reduced (Figure 2E). As expected, parental macrophages treated with LPS exhibited decreased basal and maximal respiration capacities (Figure 2D). Accordingly, parental cells treated with LPS showed reduced total and mitochondrial ATP production and increased glycolytic ATP synthesis compared to untreated cells (Figure 2E). An increasing body of evidence points to the respiratory CII as a source and modulator of ROS. Treatment with Q site inhibitors, silencing of SDHB, and mutations in SDHC-D subunits have been reported to enhance ROS generation in different mammalian cell lines and yeast.[21] Treatment with succinate-binding site inhibitors and RNA interference of SDHA, on the other hand, prevents ROS production at FAD.[12] These results provide strong evidence that FAD in SDHA is the principal site of ROS production in the mature SDH/CII. So far, in macrophages, only the indirect role of CII in LPS-induced generation of mitoROS via reverse electron transport has been described.[6] To assess ROS levels in the mitochondria, we used the mitochondria-specific ROS indicator MitoSOX to selectively detect superoxide in the mitochondria of live cells. *Sdha*−/− and *Sdhb*−/− macrophages showed higher LPS-induced mitoROS levels compared to parental cells (Figure 2F). No significant differences were observed between *Sdha*−/− and *Sdhb*−/− macrophages. These data indicate that SDH/CII does not contribute to mitoROS production in LPS-activated macrophages, although it is possible that its function may be masked by the massive production of mitoROS as a consequence of mitochondrial dysfunction or its generation from other pathways outside of the ETC. To explore the percentage of dysfunctional mitochondria, we stained mitochondria with a combination of MitoTracker Green (potential-independent dye) and MitoTracker Red (potential-dependent dye), and we observed an increase in dysfunctional mitochondria (MitoTracker Green^{+high}, MitoTracker Red^{+low}) in untreated and LPS-treated *Sdha*−/− and *Sdhb*−/− macrophages (Figure 2G). Together, these results indicate that the absence of Sdha and Sdhb severely impairs mitochondrial function by altering respiration, mitoROS accumulation, and altering $\Delta\psi m$.

Sdha and Sdhb are key players in macrophage effector functions

Pharmacological inhibition of SDHA has been reported to decrease LPS-induced IL-1β mRNA and protein expression without altering the secretion of other pro-inflammatory cytokines including IL-6 and TNF-α.[6–8] The impact of the pharmacological inhibition of SDHA is less conclusive for IL-10 as both an increase and non-significant decrease have been reported.[6–8] To clarify this matter, we next treated bone-marrow-derived macrophages (BMDMs) with the competitive SDHA inhibitor DMM. As expected, treatment with DMM attenuated the induction of IL-1β mRNA expression and IL-1β production in BMDMs treated with LPS but did not impair the secretion of TNF-α (Figure 3A). BMDMs were able to secrete IL-1β protein in response to just the priming signal LPS, albeit at low levels (Figure 3A). DMM also decreased IL-10 production in BMDMs treated with LPS. The impact of DMM on the cytokine profile of LPS-activated RAW 264.7 cells was comparable to that observed in BMDMs, supporting the suitability of RAW 264.7 cells for exploring cytokine responses (Figure 3A). Next, we examined the effects of the genetic abrogation of *Sdha* and *Sdhb* on the *cytokine* response of macrophages. We found that both *Sdha*−/− and *Sdhb*−/− exhibited decreased secretion of IL-1β after LPS stimulation as compared with parental cells (Figure 3B). The decrease in IL-1β production was more striking in *Sdhb*−/− cells than in *Sdha*−/− cells. IL-6, IFN-β, and TNF-α secretion were similar in parental, *Sdha*−/− and *Sdhb*−/− cells (Figure 3B). The greatest cytokine phenotype was found in the anti-inflammatory cytokine IL-10 (Figure 3B), which was barely detectable in the supernatants of LPS-activated *Sdha*−/− and *Sdhb*−/− cells. The decrease in IL-1β secretion in genetically modified cells was comparable to that observed in pharmacologically inhibited BMDMs and parental RAW 264.7 cells. In contrast, the defective IL-10 production was much more severe in *Sdha*−/− and *Sdhb*−/− cells than in DMM-treated macrophages. To explore whether these discrepancies in IL-10 secretion could be associated with differences in mitochondrial respiratory capacities, we explored the impact of DMM on the respiration of RAW 264.7 cells. We tested increasing doses of DMM while taking into account that 5–10 mM has been reported to be the appropriate DMM dose range to inhibit CII in macrophages.[6–8] As shown in Figure 3C, the inhibition of respiration by DMM was dose dependent and the subsequent addition of rotenone dramatically decreased OCR in all conditions. Of note, the degree of respiratory inhibition in DMM-treated cells was *considerably less than* that observed in *Sdha*- and *Sdhb*-deficient cells (Figure 2C), which might underlie their different capacity to secrete the anti-inflammatory cytokine IL-10. Macrophages represent a major source of IL-10 and recent studies have shown that macrophages themselves are the main target cells of the inhibitory IL-10 effects.[22,23] Autocrine IL-10 has been reported to act by limiting NO production and therefore preventing NO-mediated suppression of OXPHOS.[19] Not surprisingly, LPS-activated *Sdha*−/− and *Sdhb*−/− cells showed increased iNOS expression (Figure 4A) and increased nitrite accumulation in the supernatants, which are indicative of NO production (Figure 4B).

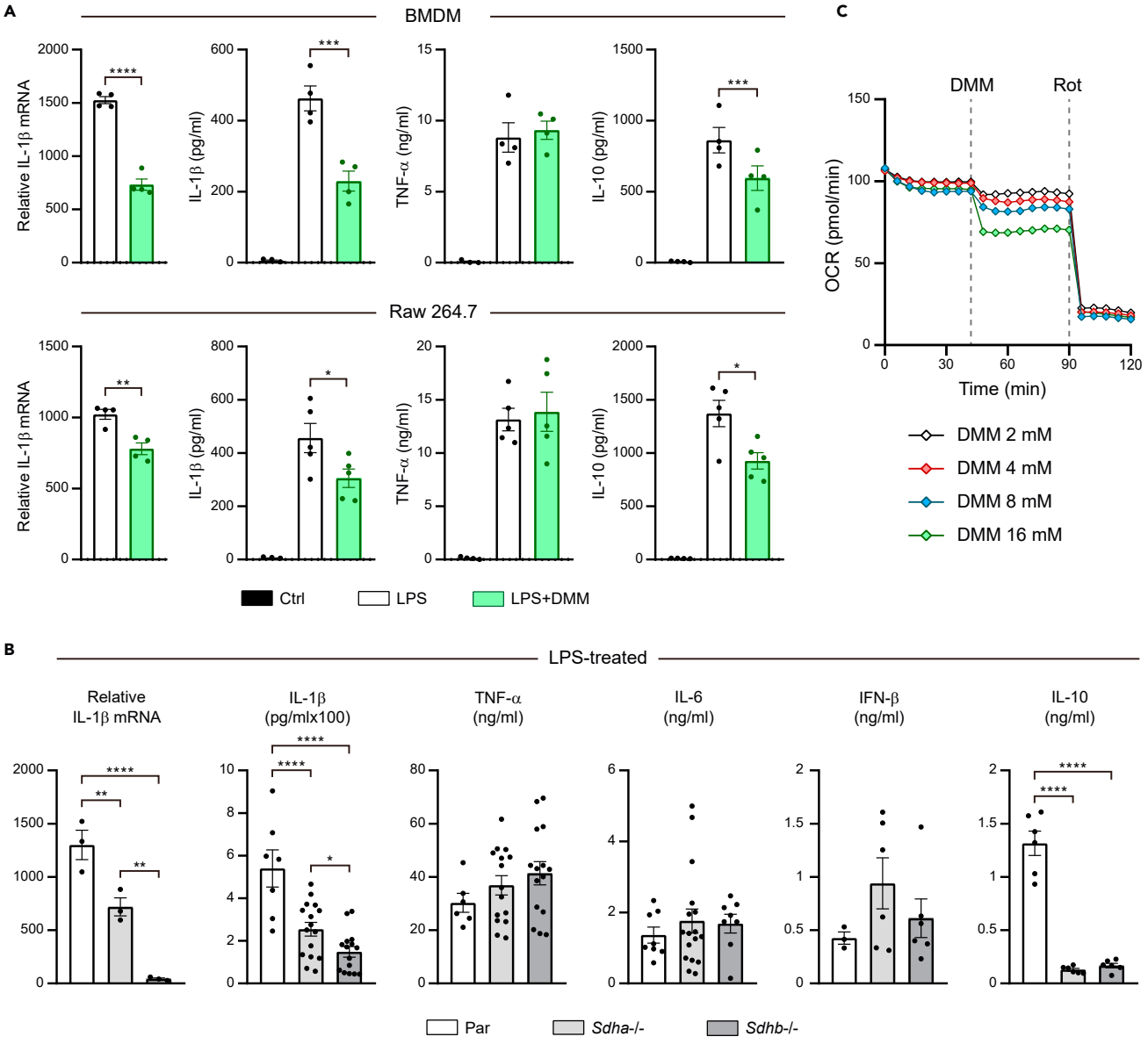

Figure 3. Role of Sdha and Sdhb in macrophage cytokine production

(A, B) BMDMs and parental (Par), *Sdha*−/− and *Sdhb*−/− RAW 264.7 cells were left untreated (control, ctrl) or treated with LPS (100 ng/mL). When indicated, cells were pretreated with DMM (16 mM) 1 h prior to stimulation with LPS. Cells were collected at 4 h for IL-1β mRNA quantification by real-time PCR (expressed as fold increases versus untreated parental cells). Supernatants were collected at 8 h for cytokines (IL-1β, TNF-α, IL-6, and IL-10) measurements by ELISA.

(C) OCR in RAW 264.7 cells was measured under basal conditions and after the sequential addition of DMM at the indicated concentrations and rotenone (Rot) (1 μM). *, $p < 0.05$; **, $p < 0.01$; ***, $p < 0.005$; ****, $p < 0.001$. Each point represents a biological replicate. Data are shown as the mean ± SEM.

To further explore the role of SDH/CII in macrophage effector functions, we investigated the ability of the cells to phagocyte fluorescently labeled *E. coli*. As shown in Figure 4C, the uptake of bacteria was significantly increased in *Sdha*−/− and *Sdhb*−/− macrophages compared to parental controls. We then estimated the bactericidal activity of the different sublines by means of the gentamicin protection assay. The number of surviving *E. coli* at time point 0 was significantly higher in the knockout cell lines than in parental control cells (Figure 4D). This result was expected, as the number of bacteria recovered from the gentamicin protection assay at early points correlates well with the phagocytic capacity. However, the bactericidal activity was unaltered in *Sdha*−/− and *Sdhb*−/− macrophages (Figure 4D). These results indicate that the absence of SDH/CII improves the ability of macrophages to clear bacteria.

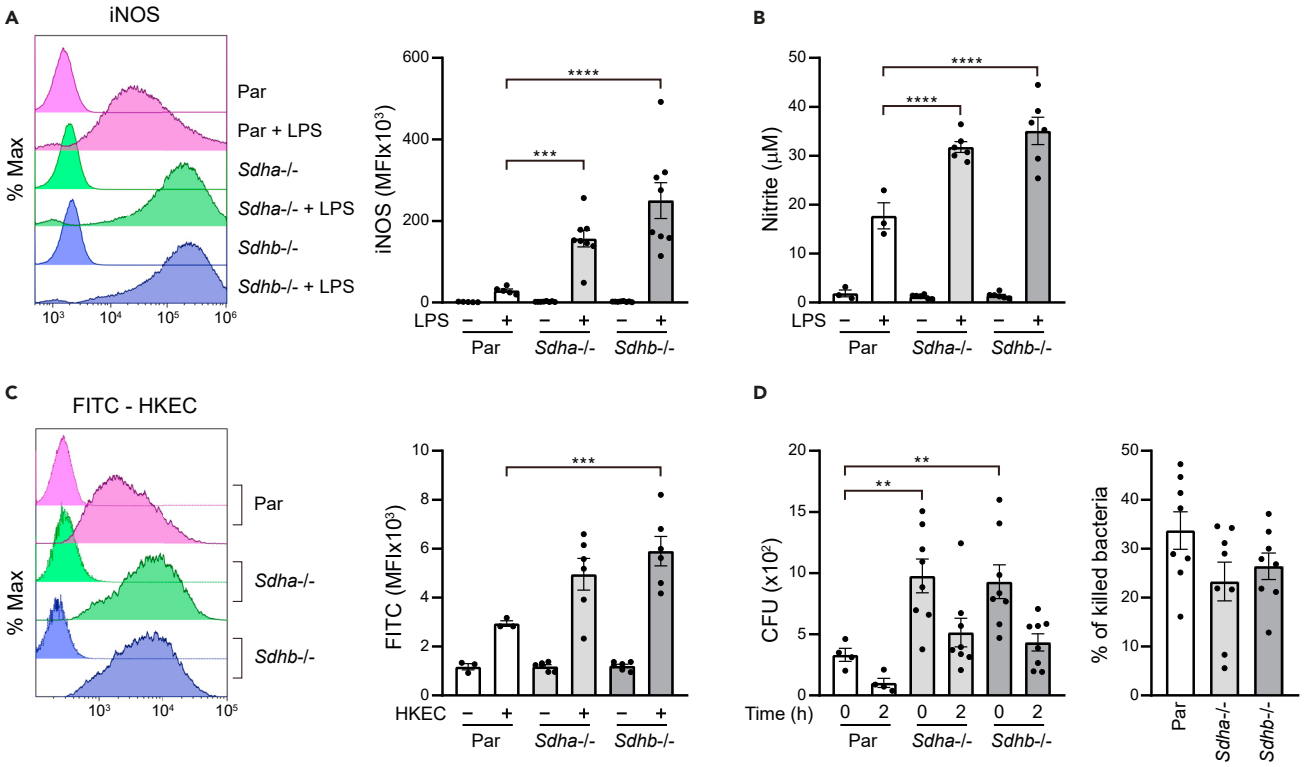

Figure 4. Role of Sdha and Sdhb in the ability of macrophages to produce NO and phagocytize and kill bacteria

(A) Representative flow cytometry histograms of iNOS staining (left) and bar graph representing the iNOS MFI values (right).

(B) Nitrite concentrations in supernatants were measured using the Griess assay. Cells were left untreated or treated with LPS (100 ng/mL) for 24 h (A, B).

(C) Representative flow cytometry plots (left) showing phagocytosis of FITC-labeled heat-killed *E. coli* and bar graph representing the MFI values (right).

(D) Bactericidal activity was measured by gentamicin protection assay. Graphs showing numbers of CFU of *E. coli* recovered at the indicated time points (left) and the percentage of killed bacteria at time point 2 h compared with time point 0 h (right). Ns, not significant; *, $p < 0.05$; **, $p < 0.01$; ***, $p < 0.005$; ****, $p < 0.001$. Each point represents a biological replicate. Data are shown as the mean ± SEM.

Sdha and Sdhb are required for induction of Stat3 transcriptional program

We next sought to determine the signaling pathways controlled by Sdha and Sdhb. HIF signaling pathways are evolutionarily conserved survival mechanisms in response to two fundamental stresses, oxygen deprivation and/or energy deficiency. In macrophages under normoxic conditions, HIF-1α can be induced by high succinate and mitoROS levels and it is necessary for IL-1β production.[4,6] In addition, succinate oxidation is necessary for HIF-1α induction as evidenced by the use of DMM, which has been shown to decrease LPS-induced HIF-1α expression and IL-1β production.[6] Here, we explored whether the absence of SDH/CII similarly impacted HIF-1α levels. As shown in Figure 5A, the expression levels of HIF-1α were significantly decreased in *Sdha−/−* and *Sdhb−/−* cells, which correlated well with the decreased secretion of IL-1β in these cells. Similarly to HIF-1α, the AMP-activated protein kinase (AMPK) is a metabolic master regulator that is activated by T172 phosphorylation when cells have an insufficient energy supply[24] or are exposed to certain stress conditions. As previously reported, LPS induced AMPK phosphorylation in parental cells[25] and as expected, the increase in pAMPK levels was significantly higher in *Sdha−/−* and *Sdhb−/−* cells (Figure 5B). AMPK activation has been reported to enhance the phagocytic ability of macrophages and neutrophils.[25] We therefore explored whether compound C, a well-known inhibitor of AMPK, was able to restore a wild-type phagocytic phenotype in the knockout cells. Treatment with compound C slightly inhibited the phagocytosis of *E. coli* in *Sdha−/−* and *Sdhb−/−* sublines, although it remained increased relative to parental cells. This demonstrates that AMPK phosphorylation only partially contributes to the enhanced phagocytosis ability of knockout cells (Figure 5C).

The inability to secrete IL-10 (Figure 3B) and to induce IL-10 transcripts (Figure S1) after LPS treatment was probably the most striking phenotypic change we observed in *Sdha−/−* and *Sdhb−/−* macrophages. IL-10 is a pleiotropic cytokine known for its potent anti-inflammatory and immunosuppressive effects.

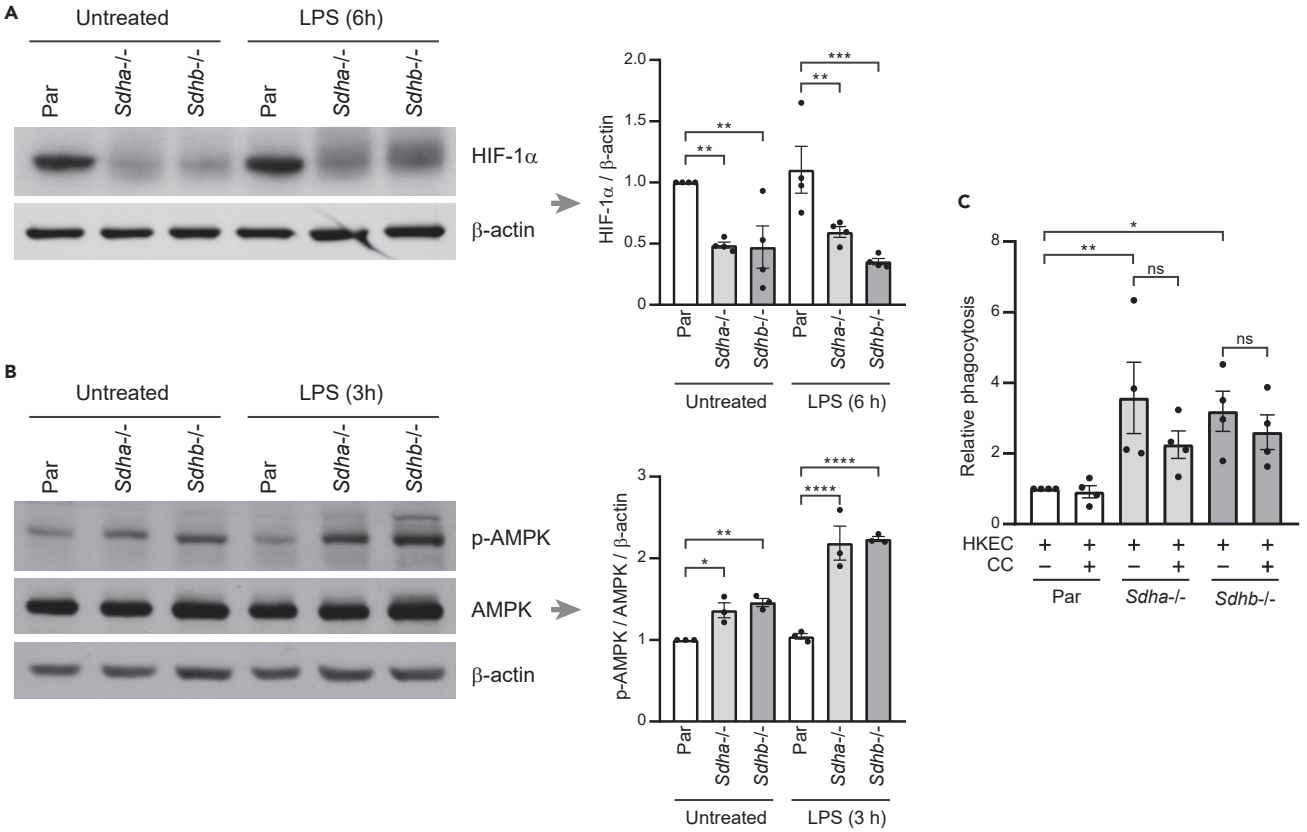

Figure 5. Metabolic signaling pathways controlled by Sdha and Sdhb

Parental (Par), *Sdha*−/− and *Sdhb*−/− RAW 264.7 cells were incubated with LPS (100 ng/mL) for the indicated times. Whole cell lysates were analyzed by Western blotting for HIF-1α (A), AMPKα pT172 and AMPKα (B), and β-actin (A and B). Relative densitometric ratios of the indicated proteins are shown in the right panels in (A) and (B).

(C) Graph showing relative phagocytosis in cells incubated with Compound C (10 μM) or vehicle for 30 min prior to the phagocytosis assays. Ns, not significant; *, $p < 0.05$; **, $p < 0.01$; ***, $p < 0.005$; ****, $p < 0.001$. Each point represents a biological replicate. Data are shown as the mean ± SEM.

In LPS-activated macrophages, autocrine IL-10 acts to resolve the inflammatory status of the cell via STAT3 signaling.[20,26] However, STAT3 activation is not simply a downstream consequence of IL-10 receptor activation, as it also participates in the induction of IL-10 gene expression in macrophages, T, and B cells.[27–29] STAT3 dimerization, which involves reciprocal binding of the STAT3-SH2 domain to phosphorylated Y705, is required for STAT3 nuclear translocation, DNA binding, and transcriptional activity. We therefore focused on examining LPS-induced Stat3 Y705 phosphorylation in the different sublines. LPS induced Stat3 Y705 phosphorylation in parental control cells (Figure 6A), as previously reported.[20] Strikingly, *Sdha* and *Sdhb* knockout dramatically decreased the levels of Stat3 pY705 (Figure 6A). Similarly, treatment with DMM attenuated the induction of Stat3 Y705 phosphorylation and IL-1β production in BMDMs treated with LPS (Figure S2).

It has been reported that autocrine IL-10 plays a crucial role in the phosphorylation of Stat3 at Y705 in macrophages treated with LPS. This was shown by experiments in which IL-10−/− macrophages and macrophages treated with neutralizing antibodies against IL-10 or IL-10R did not undergo Stat3 Y705 phosphorylation upon LPS treatment.[20,30] In our cell model, we have verified the ability of the widely used 1B1.3a neutralizing monoclonal antibody against the IL-10Rα subunit to prevent the phosphorylation of Stat3 at Y705 (Figure S3). To determine if the abolition of Stat3 Y705 phosphorylation was a consequence of the absence of IL-10 in the supernatants of the knockout sublines, we examined whether IL-10 added exogenously was able to rescue the expression of Stat3 pY705. As shown in Figure 6B, the addition of IL-10 at a high concentration (10 ng/mL) partially rescued the levels of Stat3 pY705 in LPS-treated Sdha−/− macrophages but not in LPS-treated *Sdhb*−/− macrophages. Furthermore, IL-10 (10 ng/mL) alone induced decreased levels of Stat3 pY705 in *Sdha*−/− macrophages and failed to induce Stat3 pY705 in *Sdhb*−/− macrophages (Figure 6B). We next

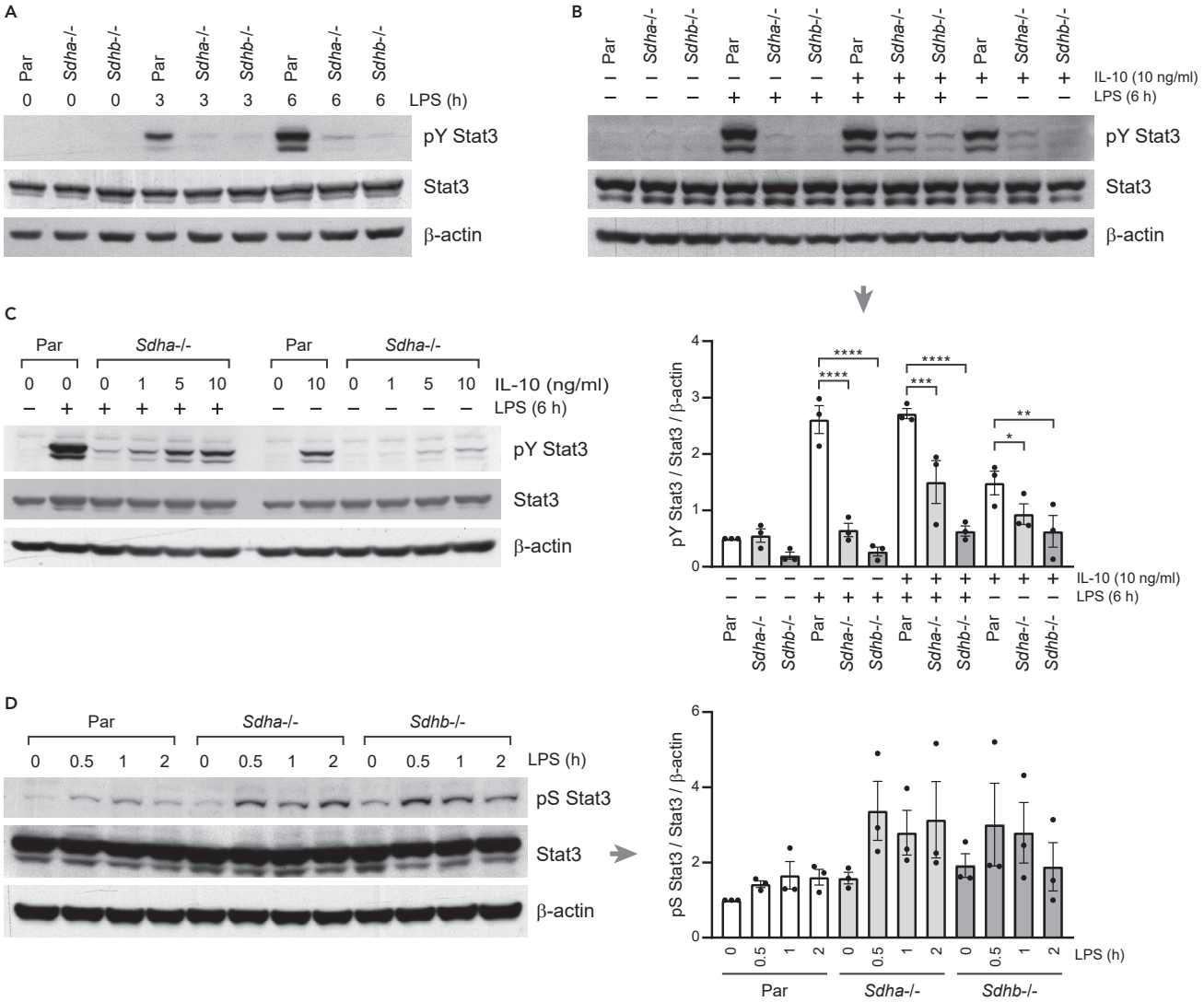

Figure 6. Role of Sdha and Sdhb in the phosphorylation and function of transcription factor Stat3

Parental, *Sdha−/−* and *Sdhb−/−* RAW 264.7 cells were left untreated or treated with 100 ng/mL LPS and/or 1–10 ng/mL IL-10 for the indicated times. Whole cell lysates were analyzed by Western blotting for Stat3 pY705 (A–C), Stat3 pS727 (D), Stat3 (A–D), and β-actin (A–D). The blots are representative of three independent experiments. Relative densitometric ratios of the indicated proteins are shown in the bottom panel in (B) and the right panel in (D). *, $p < 0.05$; **, $p < 0.01$; ***, $p < 0.005$; ****, $p < 0.001$. Each point represents a biological replicate. Data are shown as the mean ± SEM.

explored whether concentrations of IL-10 similar to those secreted by LPS-treated parental cells (1 ng/mL) were also able to partially rescue the levels of Stat3 pY705 in *Sdha−/−* macrophages. We observed that the addition of IL-10 at a concentration of 1 ng/mL was not able to rescue Stat3 Y705 phosphorylation (Figure 6C), and therefore concluded that the decreased levels of IL-10 in the supernatants of LPS-treated *Sdha−/−* are not responsible for the reduced tyrosine phosphorylation of Stat3 in these cells. Of note, in addition to IL-10, the transcripts of other anti-inflammatory STAT3 target genes were dramatically decreased, such as Arg1, Socs3, and Bcl3 (Figure S1).

In addition to Y705 phosphorylation, STAT3 protein can also be phosphorylated at S727. S727 phosphorylation has been shown to modulate the transcriptional potency of STAT3, possibly by controlling STAT3 interaction with other transcriptional cofactors.[31] S727 phosphorylation, but not Y705 phosphorylation, is also required for the functions of a small pool of STAT3 that enters the mitochondria. Mitochondrial STAT3 augments ETC activity and mitochondrial transcription independently of its functions as a nuclear transcription factor.[31] We explored whether the absence of Sdha and Sdhb also compromised the levels

of Stat3 pS727. LPS-induced Stat3 S727 phosphorylation was slightly, but not significantly, increased in *Sdha*−/− and *Sdhb*−/− macrophages compared to that observed in parental macrophages (Figure 6D). Collectively, these data demonstrate that SDH/CII is essential for Stat3 phosphorylation at Y705 but not at S727, as well as for its transcriptional activity.

The role of altered mitochondrial metabolites and mitoROS levels in the absence of Stat3 tyrosine phosphorylation in Sdha−/− and Sdhb−/− macrophages

Our subsequent aim was to investigate the molecular connection between SDH/CII and Y705 phosphorylation of Stat3. Given the growing evidence that a number of TCA metabolites control macrophage phenotypes and effector functions,[32] we hypothesized that TCA metabolites could serve as mediators in the role of SDH/CII in the anti-inflammatory Stat3/IL-10 axis. First, we examined the levels of TCA metabolites in both untreated and LPS-treated *Sdha*−/− and *Sdhb*−/− macrophages using ultra-performance liquid chromatography-mass spectrometry (Figure 7A). We found that itaconate, a metabolite known to be highly induced in LPS-activated macrophages,[33] was significantly reduced in LPS-treated *Sdha*−/− and *Sdhb*−/− macrophages. This reduction can be explained by the decrease in citrate levels. Malate levels were also decreased in these mutant macrophages both under basal conditions and after LPS treatment. On the other hand, there was a notable increase in succinate accumulation in both untreated and LPS-treated *Sdha*−/− and *Sdhb*−/− macrophages. Additionally, we observed a higher level of lactate accumulation in LPS-treated *Sdha*−/− and *Sdhb*−/− macrophages, indicative of their enhanced glycolytic phenotype. Finally, mutant macrophages showed an accumulation of oxaloacetate most likely due to increased anaplerosis. This assay was unable to detect the presence of fumarate; however, Figure 2B demonstrates that it was detected at low levels in mutant macrophages using a colorimetric assay. It is noteworthy that recent studies have highlighted the anti-inflammatory properties of itaconate and fumarate,[34–36] which are present in low quantities in *Sdha*−/− and *Sdhb*−/− macrophages. We hypothesized that itaconate and fumarate might exert anti-inflammatory effects partly via Stat3 Y705 phosphorylation, thereby providing a molecular mechanism for the absence of Y705 Stat3 phosphorylation in *Sdha*−/− and *Sdhb*−/− macrophages. Consequently, we explored whether treating the mutant macrophages with itaconate and fumarate cell-permeable derivatives could rescue the observed pY705 phenotype. As shown in Figure 7B, both 4-octyl itaconate (OI) and dimethyl fumarate (DMF) failed to rescue the pY705 phenotype in mutant cells. Furthermore, these derivatives suppressed Stat3 Y705 phosphorylation in parental cells treated with LPS. These results present preliminary evidence supporting a critical role for these metabolites in Stat3 Y705 phosphorylation. Furthermore, they indicate that the observed pY705 phenotype cannot be attributed to low levels of itaconate and fumarate.

Previous studies have indicated that excessive oxidative stress can impair the DNA-binding and transcriptional activity of STAT3 in various cell types.[37] Moreover, it has been observed that different oxidants can reduce STAT3 Y705 phosphorylation in hepatoma cells.[39] To determine whether the abolition of Stat3 Y705 phosphorylation resulted from elevated mitoROS levels in the knockout sublines, we investigated the potential of mitoTEMPO, a mitochondria-targeted ROS scavenger, to rescue Stat3 Y705 phosphorylation. As shown in Figure 7C, mitoTEMPO was able to partially restore Stat3 Y705 phosphorylation in a concentration-dependent manner. Taken together, our results reveal an important role for mitoROS in the pY705 phenotype of LPS-activated Sdha−/− and Sdhb−/− macrophages.

DISCUSSION

Attempts to define the precise role of the ETC in macrophage functions have been ongoing for the last decade. With respect to SDH/CII, the studies performed so far have been based on the use of chemical inhibitors of SDHA. In this study, we identify previously unknown roles for SDH/CII in the metabolic phenotype of macrophages and their effector functions using macrophages deficient in Sdha and Sdhb.

Our work provides evidence that the absence of Sdha and Sdhb severely impairs basal respiration in macrophages. Very similar results have been observed in other SDH knockout cell models including *Sdhb*−/− murine kidney cells,[18] *SDHB*−/− human kidney cells,[38] *SDHB*−/− human breast cancer cells,[13] and *SDHA*−/− human leukemia cells.[40] We found that both *Sdha*−/− macrophages (with no detectable levels of Sdhb) and *Sdhb*−/− macrophages (with intact Sdha expression levels) showed a similar bioenergetic pattern, indicating that free Sdha does not play a significant role in mitochondrial bioenergetics. It is noteworthy that a study using mice deficient in glycerol 3-phosphate dehydrogenase (GPD2) demonstrate that the glycerol phosphate shuttle is the major metabolic pathway that fuels ETC in LPS-activated

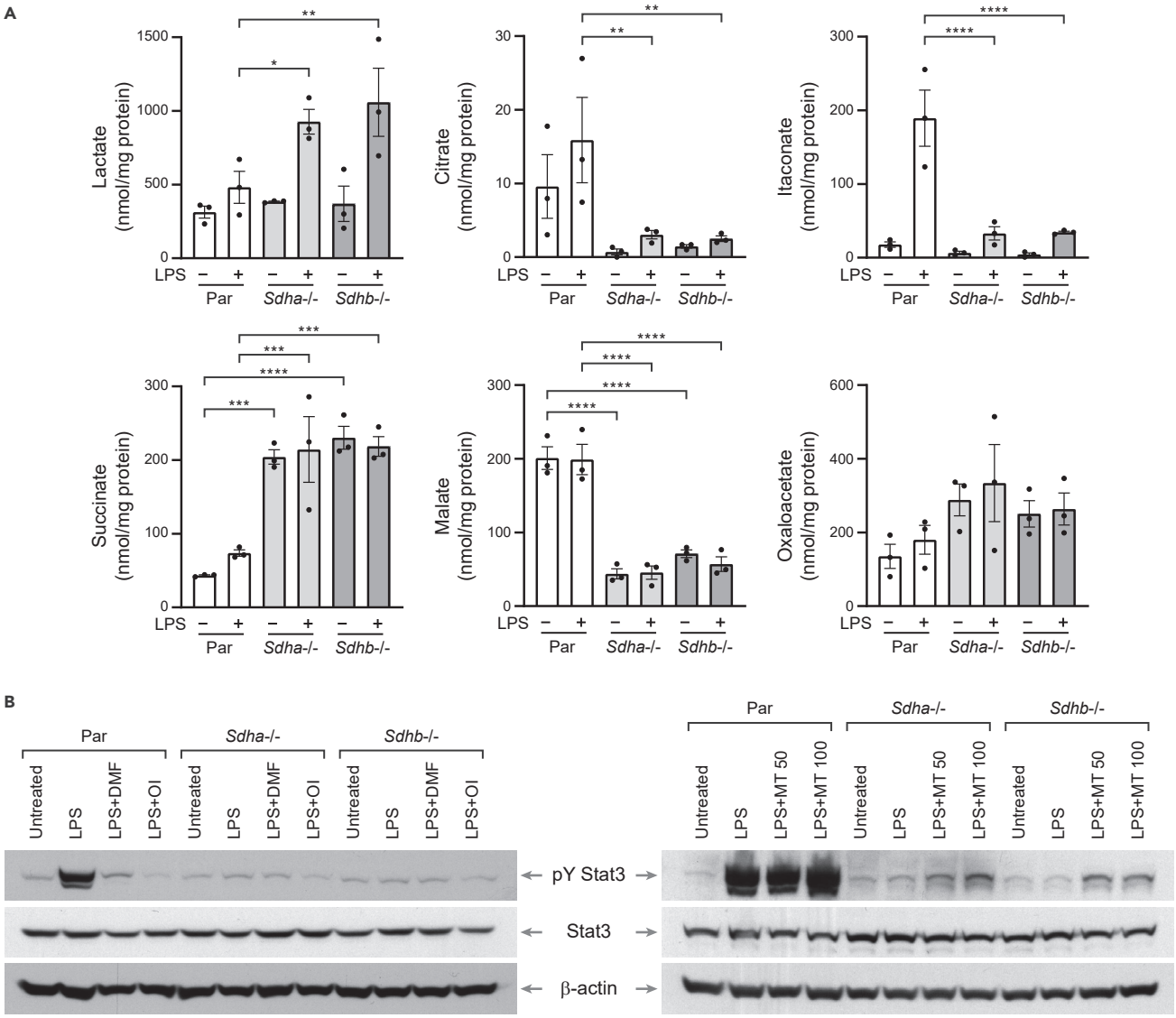

Figure 7. Assay of TCA cycle intermediates and the impact of mitoROS scavenging on Stat3 tyrosine phosphorylation in *Sdha*−/− and *Sdhb*−/− cells

(A) Parental, Sdha−/− and Sdhb−/− RAW 264.7 cells were left untreated or treated with 100 ng/mL LPS for 24 h. Thereafter, metabolites were extracted for the UPLC/MS analysis of lactate, citrate, itaconate, succinate, malate, and oxaloacetate. Fumarate and α-ketoglutarate were not detected in these assays. Each point represents a biological replicate. Data are shown as the mean ± SEM.

(B) Parental, Sdha−/− and Sdhb−/− RAW 264.7 cells were left untreated or treated with DMF (25 μM), OI (125 μM), and mitoTEMPO, abbreviated as MT (50 μM or 100 μM), for 3 h prior to stimulation with LPS (100 ng/mL). Cells were collected at 6 h after the addition of LPS and whole cell lysates were analyzed by Western blotting for Stat3 pY705, Stat3, and β-actin. The blots are representative of three independent experiments.

macrophages.[41] GPD2 is the mitochondrial component of the glycerol phosphate shuttle and couples oxidation of glycerol 3-phosphate back to dihydroxyacetone phosphate with reduction of its flavin adenine dinucleotide cofactor to FADH2, from which electrons flow downward through the ETC to drive mitochondrial respiration.[41] Collectively, these results suggest that FADH2 represents a key electron donor in both resting and LPS-activated macrophages.

Our studies also demonstrate that both SDHA and SDHB are upstream two master regulators of metabolism, HIF and AMPK. Previous reports have shown that high succinate concentrations promote the stabilization of HIF-1α and subsequent production of IL-1β in LPS-activated macrophages.[4,6] However, the metabolism of succinate by SDH is crucial for its pro-inflammatory action as demonstrated using SDHA

inhibitor DMM.[6] Our results confirm that high levels of succinate are not sufficient to elevate HIF-1α levels and promote IL-1β production, but that its further oxidation by SDH is necessary. Of note, *Sdhb*−/− macrophages behaved similarly to *Sdha*−/− macrophages, which contrasts with results obtained in cancer cell lines of different lineages showing that Sdha triggers increase in HIF-1α expression in the absence of Sdhb.[12] This finding suggests that the proposed mechanism for stabilization of HIF-1α by free SDHA in tumors with mutations in subunits SDHB, SDHC, and SDHD[12] is incomplete and that other unknown concomitant mechanisms are responsible for the increase of HIF-1α expression in SDHx tumors. The second master regulator of metabolism downstream SDH, AMPK, has been reported to enhance the phagocytic ability of macrophages.[25] Here, we demonstrate that AMPK hyperactivation underlies the increased phagocytic ability of *Sdha*−/− and *Sdhb*−/− macrophages. We have previously reported that macrophages silenced for complex I subunits NDUFS3 and NDUFS4 or treated with CI inhibitor rotenone have high phagocytic capacity, similarly to SDH-deficient cells, and the hyperactivation of AMPK was also responsible for the phagocytic phenotype.[42] AMPK has also long been recognized to have potent anti-inflammatory activity in a variety of cell types, including macrophages and epithelial cells.[43] In macrophages, AMPK has been reported to be necessary for macrophages to produce IL-10 and acquire M2 phenotype.[43] However, *Sdha*−/− and *Sdhb*−/− macrophages are unable to secrete IL-10 despite the AMPK hyperactivation, indicating that the SDH/CII target molecule responsible for the inability to produce IL-10 is downstream of the AMPK signaling pathway.

The failure to produce IL-10 is the most dramatic cytokine phenotype in *Sdha*−/− and *Sdhb*−/− macrophages. We observed that DMM treatment was also able to reduce LPS-induced IL-10 production, but to a much lesser extent. This could be because respiration is much less compromised in cells in which SDH/CII is inhibited by DMM than in knockout cells (Figure 3C). It may be also due to the fact that in knockout cells the long-term loss of SDH may be associated with metabolic adaptations that lead to lower IL-10 production. In this regard, it is important to note that a long DMM treatment of 7 days (Figure S4) causes a more significant decrease in IL-10 production than that observed with pretreatment of only 1 h (Figure 3C). Our results on IL-10 are in apparent contradiction with previous reports using SDHA chemical inhibitors, which show either an increase[6,7] or small decrease[8] in IL-10 expression. It is worth mentioning that the use of chemical inhibitors and genetic models has generated seemingly contradictory results in several cellular pathways. For example, chemical inhibition of CI impairs the production of the pro-inflammatory cytokines IL-1,[44] whereas the genetic ablation of the CI subunit NDUFS4 promotes an inflammatory macrophage phenotype.[45] This highlights the importance of combining genetic and chemical approaches for probing protein functions in cells.

In this work, we delve into the molecular mechanisms underlying the inability of *Sdha*−/− and *Sdhb*−/− macrophages to produce IL-10. We show that the SDH/CII complex is required for LPS-induced Stat3 phosphorylation at Y705, which subsequently facilitates its binding to target sequences on the IL-10 promoter and promotes transcription.[27] Furthermore, we demonstrate that the SDH/CII complex is also required for IL-10-induced Stat3 Y705 phosphorylation. Autocrine IL-10 has been reported to inhibit LPS-induced inflammatory responses of macrophages, at least in part by switching the metabolic phenotype from aerobic glycolysis to OXPHOS.[19,20,46] At the molecular level, IL-10 promotes OXPHOS by enhancing the clearance of ROS-producing mitochondria through Stat3 activation.[20] Additionally, it boosts the activity of SDH/CII by upregulating Arg2.[46] IL-10 also acts by inhibiting iNOS, thereby limiting the NO-mediated suppression of OXPHOS.[19] As expected, a low concentration of IL-10 in the culture supernatants of LPS-stimulated *Sdha*−/− and *Sdhb*−/− macrophages was associated with high iNOS expression. A previous report found that IL-10-mediated STAT3 activation represses nitric oxide synthesis.[47] Accordingly, the increased iNOS levels in *Sdha*−/− and *Sdhb*−/− macrophages were barely restored by the addition of IL-10 (Figure S5). With regard to the serine-phosphorylated form of Stat3 (pS727), we observed small but significant increase in its levels in LPS-activated *Sdha*−/− and *Sdhb*−/− macrophages. There is controversy on the biological functions and mechanism of action of Stat3 pS727. Whereas some authors have reported that Stat3 pS727 is required for maximal Stat3 transcriptional activity,[48,49] others have found that S727 phosphorylation downregulates it.[50,51] Intriguingly, STAT3 pS727 has been reported to enter the mitochondria, interact with complexes I and II, and enhance the activities of both complexes in pro-B cells.[52] Here, we present new evidence that Stat3 serine phosphorylation occurs independently of tyrosine phosphorylation and of CII integrity. However, the fact that Stat3 pS727 is slightly increased in LPS-activated *Sdha*−/− and *Sdhb*−/− macrophages may reflect the release of potential negative feedback exerted by both CII activity and Y705 phosphorylation on S727 phosphorylation.

Furthermore, our work grows the evidence for a relationship between oxidative stress and Stat3 activity and supports the notion that anti-inflammatory macrophages rely on intact mitochondria for their function.[2] The scavenging of mitoROS partially rescued Stat3 Y705 phosphorylation in LPS-activated *Sdha*−/− and *Sdhb*−/− macrophages. The partial rescue was expected given the unlikelihood that treatment with mito-TEMPO would effectively reverse the extensive molecular changes (i.e., epigenetic alterations, post-translational modifications) resulting from chronic oxidative stress. Our work also demonstrates that reduced levels of itaconate and fumarate in *Sdha*−/− and *Sdhb*−/− macrophages do not play a role in the pY705 phenotype. In addition, we show that cell-permeable derivatives OI and DMF, used at standard concentrations,[34,35] strongly inhibit Stat3 Y705 tyrosine phosphorylation in LPS-treated parental cells. To date, the documented effects of these metabolites have primarily focused on their anti-inflammatory properties. In particular, their ability to inhibit IL-1β secretion has been extensively investigated.[34–36] Remarkably, itaconate has been shown to suppress the HIF-1α/IL-1β pathway, partly through its ability to inhibit SDH activity.[54]

Lastly, we would like to discuss the apparent lack of phenotypic differences between *Sdha*−/− and *Sdhb*−/− macrophages. As summarized in the introduction section, the free SDHA subunit in SDHB-silenced cells has been proposed as a tumor driver by increasing HIF-1α stabilization and promoting cell growth.[12] Accordingly, SDHA-silenced cells showed decreased HIF-1α levels and growth rates.[12] However, we observed decreased HIF-1α protein levels in both *Sdha*−/− and *Sdhb*−/− macrophages. Moreover, we observed decreased growth rates in both deficient cell lines (Figure S6). Our finding is in line with a more recent report that also describes decreased growth rates in human breast cancer cell line deficient in SDHB. This report explains that, in the absence of SDHB, the role of SDHA in promoting cell growth is not detectable under normal conditions, but rather under nutrient-poor conditions.[13] Also, in line with our results, Armstrong has shown that the ablation of *Sdhb* only initiates tumorigenesis in mouse chromaffin cells when there is a concomitant loss of *Nf1*.[14]

In conclusion, our work provides new insights into the role of the ETC in controlling macrophage immunometabolism and effector functions, contributing to the growing body of knowledge on the function of the mitochondria in immune system functions.

Limitations of the study

The main finding of this study indicates that SDH/CII controls the Stat3-IL-10 pathway in inflammatory macrophages. Investigating the precise mechanisms by which SDH/CII controls Stat3 Y705 phosphorylation was challenging, particularly because mitochondria of *Sdha*−/− and *Sdhb*−/− macrophages are highly dysfunctional. This dysfunction leads to excessive and persistent oxidative stress, resulting in stable structural modifications of cellular proteins and simultaneous alterations in multiple signaling pathways. Future studies using inducible *Sdha*−/− and *Sdhb*−/− macrophages will help to explore the direct effects of SDH/CII ablation on effector functions.

STAR★METHODS

Detailed methods are provided in the online version of this paper and include the following:

- KEY RESOURCES TABLE
- RESOURCE AVAILABILITY
  - Lead contact
  - Materials availability
  - Data and code availability
- EXPERIMENTAL MODEL AND STUDY PARTICIPANT DETAILS
  - Cell lines
  - Mice
- METHOD DETAILS
  - Plasmids construction
  - Generation of *Sdha*−/− and *Sdhb*−/− macrophages
  - Complex II activity
  - Seahorse metabolic analysis
  - Measurement of cytokines and nitric oxide (NO)
  - Phagocytosis and bacterial killing assays

- Flow cytometry
- Real-time PCR
- Western blotting
- Extraction and assay of metabolites

- QUANTIFICATION AND STATISTICAL ANALYSIS
- ADDITIONAL RESOURCES

SUPPLEMENTAL INFORMATION

Supplemental information can be found online at https://doi.org/10.1016/j.isci.2023.107473.

ACKNOWLEDGMENTS

Funding information: Agencia Estatal de Investigación, Grant Number PID2020-118517RB-I00; Consejería de Educación, Junta de Castilla y León, Grant Number VA172P20; Consejería de Sanidad, Junta de Castilla y León, Grant Number GRS 2201/A/2020; Programa Estratégico Instituto de Biología y Genética Molecular (IBGM), Junta de Castilla y León, Award Number CCVC8485; Switzerland National Science Foundation, Grant Number 310030_200796. We thank the Flow Cytometry Core Facility at the unit of Excellence Institute of Biology and Molecular Genetics (IBGM), University of Valladolid-CSIC, for flow cytometry analysis, and the Animal Core Facility at the Medical School of the University of Valladolid for maintenance of the mouse colony. We also thank Olimpio Montero, Joan Blanco-Fernandez, and Chloé Chapuis for assistance.

AUTHOR CONTRIBUTIONS

Conceptualization, M.S. and M.d.F.; Methodology, D.G., P.S., M.J.E.-A., J.S.; Investigation, D.G., P.S., M.J.E.-A., J.S., M.T.P.-G., M.A.d.l.F., M.S.; Writing-Original Draft, M.S., M.A.d.l.F.; Writing-Review & Editing, M.T.P.-G., A.O., M.A.M.-C., M.A.d.l.F., M.S.; Visualization, D.G., M.S., M.A.d.l.F.; Supervision, A.O., M.A.M.-C., M.A.d.l.F., M.S.; Funding Acquisition, M.T.P.-G., A.O., M.A.M.-C., M.A.d.l.F., M.S.

DECLARATION OF INTERESTS

The authors declare no competing interests.

INCLUSION AND DIVERSITY

We support inclusive, diverse, and equitable conduct of research.

Received: December 15, 2022
Revised: February 17, 2023
Accepted: July 21, 2023
Published: July 25, 2023

REFERENCES

1. Dard, L., Blanchard, W., Hubert, C., Lacombe, D., and Rossignol, R. (2020). Mitochondrial functions and rare diseases. Mol. Aspect. Med. *71*, 100842. https://doi.org/10.1016/J.MAM.2019.100842.

2. Viola, A., Munari, F., Sánchez-Rodríguez, R., Scolaro, T., and Castegna, A. (2019). The Metabolic Signature of Macrophage Responses. Front. Immunol. *10*, 1462. https://doi.org/10.3389/FIMMU.2019.01462.

3. Liu, Y., Xu, R., Gu, H., Zhang, E., Qu, J., Cao, W., Huang, X., Yan, H., He, J., and Cai, Z. (2021). Metabolic reprogramming in macrophage responses. Biomark. Res. *9*, 1. https://doi.org/10.1186/S40364-020-00251-Y.

4. Tannahill, G.M., Curtis, A.M., Adamik, J., Palsson-Mcdermott, E.M., McGettrick, A.F., Goel, G., Frezza, C., Bernard, N.J., Kelly, B., Foley, N.H., et al. (2013). Succinate is a danger signal that induces IL-1β via HIF-1α. Nature *496*, 238–242. https://doi.org/10.1038/NATURE11986.

5. Jha, A.K., Huang, S.C.C., Sergushichev, A., Lampropoulou, V., Ivanova, Y., Loginicheva, E., Chmielewski, K., Stewart, K.M., Ashall, J., Everts, B., et al. (2015). Network integration of parallel metabolic and transcriptional data reveals metabolic modules that regulate macrophage polarization. Immunity *42*, 419–430. https://doi.org/10.1016/J.IMMUNI.2015.02.005.

6. Mills, E.L., Kelly, B., Logan, A., Costa, A.S.H., Varma, M., Bryant, C.E., Tourlomousis, P., Däbritz, J.H.M., Gottlieb, E., Latorre, I., et al. (2016). Succinate Dehydrogenase Supports Metabolic Repurposing of Mitochondria to Drive Inflammatory Macrophages. Cell *167*, 457–470.e13. https://doi.org/10.1016/j.cell.2016.08.064.

7. Garaude, J., Acín-Pérez, R., Martínez-Cano, S., Enamorado, M., Ugolini, M., Nistal-Villán, E., Hervás-Stubbs, S., Pelegrín, P., Sander, L.E., Enríquez, J.A., and Sancho, D. (2016). Mitochondrial respiratory-chain adaptations in macrophages contribute to antibacterial host defense. Nat. Immunol. *17*, 1037–1045. https://doi.org/10.1038/ni.3509.

8. Billingham, L.K., Stoolman, J.S., Vasan, K., Rodriguez, A.E., Poor, T.A., Szibor, M., Jacobs, H.T., Reczek, C.R., Rashidi, A., Zhang, P., et al. (2022). Mitochondrial electron transport chain is necessary for NLRP3 inflammasome activation. Nat. Immunol. *23*, 692–704. https://doi.org/10.1038/S41590-022-01185-3.

9. Bezawork-Geleta, A., Rohlena, J., Dong, L., Pacak, K., and Neuzil, J. (2017). Mitochondrial Complex II: At the Crossroads. Trends Biochem. Sci. *42*, 312–325. https://doi.org/10.1016/j.tibs.2017.01.003.

10. Fullerton, M., McFarland, R., Taylor, R.W., and Alston, C.L. (2020). The genetic basis of isolated mitochondrial complex II deficiency. Mol. Genet. Metabol. *131*, 53–65. https://doi.org/10.1016/J.YMGME.2020.09.009.

11. Benn, D.E., Gimenez-Roqueplo, A.-P., Reilly, J.R., Bertherat, J., Burgess, J., Byth, K., Croxson, M., M Dahia, P.L., Elston, M., Gimm, O., et al. (2006). Clinical Presentation and Penetrance of Pheochromocytoma/Paraganglioma Syndromes. https://doi.org/10.1210/jc.2005-1862.

12. Guzy, R.D., Sharma, B., Bell, E., Chandel, N.S., and Schumacker, P.T. (2008). Loss of the SdhB, but Not the SdhA, Subunit of Complex II Triggers Reactive Oxygen Species-Dependent Hypoxia-Inducible Factor Activation and Tumorigenesis. Mol. Cell Biol. *28*, 718–731. https://doi.org/10.1128/MCB.01338-07.

13. Bezawork-Geleta, A., Wen, H., Dong, L., Yan, B., Vider, J., Boukalova, S., Krobova, L., Vanova, K., Zobalova, R., Sobol, M., et al. (2018). Alternative assembly of respiratory complex II connects energy stress to metabolic checkpoints. Nat. Commun. *9*, 2221. https://doi.org/10.1038/s41467-018-04603-z.

14. Armstrong, N., Storey, C.M., Noll, S.E., Margulis, K., Soe, M.H., Xu, H., Yeh, B., Fishbein, L., Kebebew, E., Howitt, B.E., et al. (2022). SDHB knockout and succinate accumulation are insufficient for tumorigenesis but dual SDHB/NF1 loss yields SDHx-like pheochromocytomas. Cell Rep. *38*, 110453. https://doi.org/10.1016/j.celrep.2022.110453.

15. Suzuki, K., Tsunekawa, Y., Hernandez-benitez, R., Wu, J., Zhu, J., Kim, E.J., Hatanaka, F., Yamamoto, M., Araoka, T., Li, Z., et al. (2016). In Vivo Genome Editing via CRISPR/Cas9 Mediated Homology-independent Targeted Integration. https://doi.org/10.1038/nature20565.

16. Medja, F., Allouche, S., Frachon, P., Jardel, C., Malgat, M., Mousson De Camaret, B., Slama, A., Lunardi, J., Mazat, J.P., and Lombès, A. (2009). Development and Implementation of Standardized Respiratory Chain Spectrophotometric Assays for Clinical Diagnosis. https://doi.org/10.1016/j.mito.2009.05.001.

17. Maklashina, E., Rajagukguk, S., Iverson, T.M., and Cecchini, G. (2018). The unassembled flavoprotein subunits of human and bacterial complex II have impaired catalytic activity and generate only minor amounts of ROS. J. Biol. Chem. *293*, 7754–7765. https://doi.org/10.1074/JBC.RA118.001977.

18. Cardaci, S., Zheng, L., Mackay, G., Van Den Broek, N.J.F., Mackenzie, E.D., Nixon, C., Stevenson, D., Tumanov, S., Bulusu, V., Kamphorst, J.J., et al. (2015). Pyruvate carboxylation enables growth of SDH-deficient cells by supporting aspartate biosynthesis. Nat. Cell Biol. *17*, 1317–1326. https://doi.org/10.1038/ncb3233.

19. Baseler, W.A., Davies, L.C., Quigley, L., Ridnour, L.A., Weiss, J.M., Hussain, S.P., Wink, D.A., and McVicar, D.W. (2016). Autocrine IL-10 functions as a rheostat for M1 macrophage glycolytic commitment by tuning nitric oxide production. Redox Biol. *10*, 12–23. https://doi.org/10.1016/J.REDOX.2016.09.005.

20. Ip, W.K.E., Hoshi, N., Shouval, D.S., Snapper, S., and Medzhitov, R. Anti-inflammatory effect of IL-10 mediated by metabolic reprogramming of macrophages. 10.1126/science.aal3535

21. Hadrava Vanova, K., Kraus, M., Neuzil, J., and Rohlena, J. (2020). Mitochondrial Complex II and Reactive Oxygen Species in Disease and Therapy, pp. 26–32. https://doi.org/10.1080/13510002.2020.1752002.

22. Shouval, D.S., Biswas, A., Goettel, J.A., McCann, K., Conaway, E., Redhu, N.S., Mascanfroni, I.D., AlAdham, Z., Lavoie, S., Ibourk, M., et al. (2014). Interleukin-10 Receptor Signaling in Innate Immune Cells Regulates Mucosal Immune Tolerance and Anti-Inflammatory Macrophage Function. Immunity *40*, 706–719. https://doi.org/10.1016/J.IMMUNI.2014.03.011.

23. Zigmond, E., Bernshtein, B., Friedlander, G., Walker, C.R., Yona, S., Kim, K.W., Brenner, O., Krauthgamer, R., Varol, C., Müller, W., and Jung, S. (2014). Macrophage-restricted interleukin-10 receptor deficiency, but not IL-10 deficiency, causes severe spontaneous colitis. Immunity *40*, 720–733. https://doi.org/10.1016/J.IMMUNI.2014.03.012.

24. Geiß, C., Salas, E., Guevara-Coto, J., Régnier-Vigouroux, A., and Mora-Rodríguez, R.A. (2022). Multistability in Macrophage Activation Pathways and Metabolic Implications. Cells *11*. https://doi.org/10.3390/CELLS11030404.

25. Bae, H.-B., Zmijewski, J.W., Deshane, J.S., Tadie, J.-M., Chaplin, D.D., Takashima, S., Abraham, E., -Bae, H.-B., Chaplin, J.-M., and Abraham, S. AMP-activated protein kinase enhances the phagocytic ability of macrophages and neutrophils. 10.1096/fj.11-190587

26. O'Farrell, A.M., Liu, Y., Moore, K.W., and Mui, A.L. (1998). IL-10 inhibits macrophage activation and proliferation by distinct signaling mechanisms: evidence for Stat3-dependent and-independent pathways. EMBO J. *17*, 1006–1018.

27. Benkhart, E.M., Siedlar, M., Wedel, A., Werner, T., and Ziegler-Heitbrock, H.W. (2000). Role of Stat3 in Lipopolysaccharide-Induced IL-10 Gene Expression. J. Immunol. *165*, 1612–1617. https://doi.org/10.4049/JIMMUNOL.165.3.1612.

28. Hedrich, C.M., Rauen, T., Apostolidis, S.A., Grammatikos, A.P., Rodriguez Rodriguez, N., Ioannidis, C., Kyttaris, V.C., Crispin, J.C., and Tsokos, G.C. (2014). Stat3 promotes IL-10 expression in lupus T cells through trans-activation and chromatin remodeling. Proc. Natl. Acad. Sci. USA *111*, 13457–13462. https://doi.org/10.1073/PNAS.1408023111.

29. Jaslow, S.L., Gibbs, K.D., Fricke, W.F., Wang, L., Pittman, K.J., Mammel, M.K., Thaden, J.T., Fowler, V.G., Hammer, G.E., Elfenbein, J.R., and Ko, D.C. (2018). Salmonella Activation of STAT3 Signaling by SarA Effector Promotes Intracellular Replication and Production of IL-10. Cell Rep. *23*, 3525–3536. https://doi.org/10.1016/J.CELREP.2018.05.072.

30. Carl, V.S., Gautam, J.K., Comeau, L.D., and Smith, M.F. (2004). Role of endogenous IL-10 in LPS-induced STAT3 activation and IL-1 receptor antagonist gene expression. J. Leukoc. Biol. *76*, 735–742. https://doi.org/10.1189/JLB.1003526.

31. Huynh, J., Chand, A., Gough, D., and Ernst, M. Therapeutically Exploiting STAT3 Activity in Cancer — Using Tissue Repair as a Road Map. 10.1038/s41568-018-0090-8

32. Noe, J.T., and Mitchell, R.A. (2019). Tricarboxylic acid cycle metabolites in the control of macrophage activation and effector phenotypes. J. Leukoc. Biol. *106*, 359–367. https://doi.org/10.1002/JLB.3RU1218-496R.

33. Strelko, C.L., Lu, W., Dufort, F.J., Seyfried, T.N., Chiles, T.C., Rabinowitz, J.D., and Roberts, M.F. (2011). Itaconic Acid Is a Mammalian Metabolite Induced during Macrophage Activation. J. Am. Chem. Soc. *133*, 16386–16389. https://doi.org/10.1021/ja2070889.

34. Hooftman, A., Angiari, S., Hester, S., Corcoran, S.E., Runtsch, M.C., Ling, C., Ruzek, M.C., Slivka, P.F., McGettrick, A.F., Banahan, K., et al. (2020). The Immunomodulatory Metabolite Itaconate Modifies NLRP3 and Inhibits Inflammasome Activation. Cell Metabol. *32*, 468–478.e7. https://doi.org/10.1016/J.CMET.2020.07.016.

35. Hoyle, C., Green, J.P., Allan, S.M., Brough, D., and Lemarchand, E. (2022). Itaconate and fumarate derivatives inhibit priming and activation of the canonical NLRP3 inflammasome in macrophages. Immunology *165*, 460–480. https://doi.org/10.1111/IMM.13454.

36. Bambouskova, M., Potuckova, L., Paulenda, T., Kerndl, M., Mogilenko, D.A., Lizotte, K., Swain, A., Hayes, S., Sheldon, R.D., Kim, H., et al. (2021). Itaconate confers tolerance to late NLRP3 inflammasome activation. Cell Rep. *34*, 108756. https://doi.org/10.1016/J.CELREP.2021.108756.

37. Chun, K.S., Jang, J.H., and Kim, D.H. (2020). Perspectives Regarding the Intersections between STAT3 and Oxidative Metabolism in Cancer. Cells *9*, 2202–2217. https://doi.org/10.3390/CELLS9102202.

38. Saxena, N., Maio, N., Crooks, D.R., Ricketts, C.J., Yang, Y., Wei, M.H., Fan, T.W.M., Lane, A.N., Sourbier, C., Singh, A., et al. (2016). SDHB-Deficient Cancers: The Role of Mutations That Impair Iron Sulfur Cluster Delivery. J. Natl. Cancer Inst. *108*, 287. https://doi.org/10.1093/JNCI/DJV287.

39. Xie, Y., Kole, S., Precht, P., Pazin, M.J., and Bernier, M. (2009). S-Glutathionylation Impairs Signal Transducer and Activator of Transcription 3 Activation and Signaling. Endocrinology *150*, 1122–1131. https://doi.org/10.1210/EN.2008-1241.

40. Lorendeau, D., Rinaldi, G., Boon, R., Spincemaille, P., Metzger, K., Jäger, C., Christen, S., Dong, X., Kuenen, S., Voordeckers, K., et al. (2017). Dual loss of succinate dehydrogenase (SDH) and complex I activity is necessary to recapitulate the metabolic phenotype of SDH mutant tumors. Metab. Eng. *43*, 187–197. https://doi.org/10.1016/J.YMBEN.2016.11.005.

41. Langston, P.K., Nambu, A., Jung, J., Shibata, M., Aksoylar, H.I., Lei, J., Xu, P., Doan, M.T., Jiang, H., MacArthur, M.R., et al. (2019). Glycerol phosphate shuttle enzyme GPD2 regulates macrophage inflammatory responses. Nat. Immunol. *20*, 1186–1195. https://doi.org/10.1038/S41590-019-0453-7.

42. García Del Río, A., Delmiro, A., Martín, M.A., Cantalapiedra, R., Carretero, R., Durántez, C., Menegotto, F., Morán, M., Serrano-Lorenzo, P., De la Fuente, M.A., et al. (2018). The Mitochondrial Isoform of FASTK Modulates Nonopsonic Phagocytosis of Bacteria by Macrophages via Regulation of Respiratory Complex I. J. Immunol. *201*, 2977–2985. https://doi.org/10.4049/JIMMUNOL.1701075.

43. Guragain, D., Gurung, P., Chang, J.H., Katila, N., Chang, H.W., Jeong, B.S., Choi, D.Y., and Kim, J.A. (2020). AMPK is essential for IL-10 expression and for maintaining balance between inflammatory and cytoprotective signaling. Biochim. Biophys. Acta, Gen. Subj. *1864*, 129631. https://doi.org/10.1016/j.bbagen.2020.129631.

44. Kelly, B., Tannahill, G.M., Murphy, M.P., and O'Neill, L.A.J. (2015). Metformin Inhibits the Production of Reactive Oxygen Species from NADH:Ubiquinone Oxidoreductase to Limit Induction of Interleukin-1β (IL-1β) and Boosts Interleukin-10 (IL-10) in Lipopolysaccharide (LPS)-activated Macrophages. J. Biol. Chem. *290*, 20348–20359. https://doi.org/10.1074/JBC.M115.662114.

45. Jin, Z., Wei, W., Yang, M., Du, Y., and Wan, Y. (2014). Mitochondrial Complex I Activity Suppresses Inflammation and Enhances Bone Resorption by Tipping the Balance of Macrophage-Osteoclast Polarization. Cell Metabol. *20*, 483–498. https://doi.org/10.1016/J.CMET.2014.07.011.

46. Dowling, J.K., Afzal, R., Gearing, L.J., Cervantes-Silva, M.P., Annett, S., Davis, G.M., De Santi, C., Assmann, N., Dettmer, K., Gough, D.J., et al. (2021). Mitochondrial arginase-2 is essential for IL-10 metabolic reprogramming of inflammatory macrophages. Nat. Commun. *12*, 1–14. https://doi.org/10.1038/s41467-021-21617-2.

47. Queval, C.J., Song, O.-R., Deboosère, N., Delorme, V., Debrie, A.-S., Iantomasi, R., Veyron-Churlet, R., Jouny, S., Redhage, K., Deloison, G., et al. (2016). STAT3 Represses Nitric Oxide Synthesis in Human Macrophages upon Mycobacterium tuberculosis Infection OPEN. https://doi.org/10.1038/srep29297.

48. Zhang, X., Blenis, J., Li, H.C., Schindler, C., and Chen-Kiang, S. (1995). Requirement of Serine Phosphorylation for Formation of STAT-Promoter Complexes. Science 84 *267*, 1990–1994. https://doi.org/10.1126/SCIENCE.7701321.

49. Wen, Z., Zhong, Z., and Darnell, J.E. (1995). Maximal activation of transcription by Stat1 and Stat3 requires both tyrosine and serine phosphorylation. Cell *82*, 241–250. https://doi.org/10.1016/0092-8674(95)90311-9.

50. Chung, J., Uchida, E., Grammer, T.C., and Blenis, J. (1997). STAT3 serine phosphorylation by ERK-dependent and -independent pathways negatively modulates its tyrosine phosphorylation. Mol. Cell Biol. *17*, 6508–6516. https://doi.org/10.1128/MCB.17.11.6508.

51. Lim, C.P., and Cao, X. (1999). Serine phosphorylation and negative regulation of Stat3 by JNK. J. Biol. Chem. *274*, 31055–31061. https://doi.org/10.1074/JBC.274.43.31055.

52. Wegrzyn, J., Potla, R., Chwae, Y.J., Sepuri, N.B.V., Zhang, Q., Koeck, T., Derecka, M., Szczepanek, K., Szelag, M., Gornicka, A., et al. (2009). Function of Mitochondrial Stat3 in Cellular Respiration. Science *323*, 793–797. https://doi.org/10.1126/SCIENCE.1164551.

53. Morán, M., Rivera, H., Sánchez-Aragó, Blázquez, A., Merinero, B., Ugalde, C., Arenas, J., Cuezva, J.M., and Martín, M.A. (2010). Mitochondrial bioenergetics and dynamics interplay in complex I-deficient fibroblasts. Biochim. Biophys. Acta, Mol. Basis Dis. 1802, 443–453. https://doi.org/10.1016/J.BBADIS.2010.02.001.

54. Vicky Lampropoulou, A., Sergushichev, A., Bambouskova, M., Diwan, A., Diamond, M.S., Artyomov Correspondence, M.N., Lampropoulou, V., Nair, S., Vincent, E.E., Loginicheva, E., et al. (2016). Itaconate Links Inhibition of Succinate Dehydrogenase with Macrophage Metabolic Remodeling and Regulation of Inflammation Cell Metabolism Itaconate Links Inhibition of Succinate Dehydrogenase with Macrophage Metabolic Remodeling and Regulation of Inflamm. https://doi.org/10.1016/j.cmet.2016.06.004.

55. Márquez, S., Fernández, J.J., Mancebo, C., Herrero-Sánchez, C., Ferná Ndez, N., Sá Nchez, M., Rodríguez Prados, M., Cubillos-Ruiz, J.R., Montero, O., Fernández, N., and Sánchez Crespo, M. (2019). Tricarboxylic Acid Cycle Activity and Remodeling of Glycerophosphocholine Lipids Support Cytokine Induction in Response to Fungal Patterns. Cell Rep. *27*, 525–536.e4. https://doi.org/10.1016/j.celrep.2019.03.033.

56. Kurczy, M.E., Forsberg, E.M., Thorgersen, M.P., Poole, F.L., Benton, H.P., Ivanisevic, J., Tran, M.L., Wall, J.D., Elias, D.A., Adams, M.W.W., and Siuzdak, G. (2016). Global Isotope Metabolomics Reveals Adaptive Strategies for Nitrogen Assimilation. ACS Chem. Biol. *11*, 1677–1685. https://doi.org/10.1021/ACSCHEMBIO.6B00082/SUPPL_FILE/CB6B00082_SI_001.PDF.

STAR★METHODS

KEY RESOURCES TABLE

REAGENT or RESOURCE	SOURCE	IDENTIFIER
Antibodies		
iNOS Monoclonal Antibody (CXNFT), APC	Thermo Fisher Scientific	Cat#17-5920-82; RRID:AB_2573244
Monoclonal antibody anti-β-actin-peroxidase	Sigma-Aldrich	Cat#A3854; RRID:AB_262011
Rabbit polyclonal anti-AMPKα	Cell Signaling	Cat#2532; RRID:AB_330331
Rabbit polyclonal anti-Phospho-AMPKα (Thr172)	Cell Signaling	Cat#2531; RRID:AB_330330
Rat Monoclonal anti-CD210/IL-10R (1B1.3a)	Thermo Fisher Scientific	Cat# 16-2101-85; RRID:AB_2573082
Rabbit polyclonal anti-HIF-1α	Novus Biologicals	Cat#NB100-449
Mouse monoclonal anti-SDHA (B-1)	Santa Cruz Biotechnology, Inc.	Cat#sc-166909; RRID:AB_10611174
Mouse monoclonal anti-SDHB (21A11AE7)	Thermo Fisher Scientific	Cat#459230; RRID:AB_2532233
Rabbit polyclonal anti-Stat3	Cell Signaling	Cat#9132; RRID: AB_331588
Mouse monoclonal anti-Phospho-Stat3 (Ser727)	Cell Signaling	Cat#9136; RRID:AB_331755
Rabbit polyclonal anti-Phospho-Stat3 (Tyr705)	Cell Signaling	Cat#9131; RRID: AB_331586
Bacterial and virus strains		
Escherichia coli DH5α	Thermo Fisher Scientific	Cat#18258012;
Chemicals, peptides, and recombinant proteins		
BamHI	Thermo Fisher Scientific	Cat#ER0051
BbsI	Thermo Fisher Scientific	Cat#ER1012
SalI	Thermo Fisher Scientific	Cat#ER0641
TrueCut Cas9 Protein v2	Thermo Fisher Scientific	Cat#A36498
Decylubiquinone	Sigma-Aldrich	Cat#D7911; CAS: 55486-00-5
2,6-Dichloroindophenol sodium salt hydrate	Sigma-Aldrich	Cat#D1878; CAS: 1266615-56-8
Antimycin A	Sigma-Aldrich	Cat# A8674; CAS: 1397-94-0
Carbonyl cyanide 4-(trifluoromethoxy) phenylhydrazone (FCCP)	Sigma-Aldrich	Cat#C2920; CAS: 370-86-5
Compound C, AMPK Inhibito	Sigma-Aldrich	Cat#171260; CAS: 866405-64-3
Dimethyl fumarate	Thermo Fisher Scientific	Cat#11324489; CAS: 624-49-7
Dimethyl malonate	Thermo Fisher Scientific	Cat#A11007; CAS: 108-59-8
Oligomycin A	Sigma-Aldrich	Cat#75351; CAS: 579-13-5
Rotenone	Sigma-Aldrich	Cat#R8875; CAS: 83-79-4
2-Deoxy-D-glucose	Sigma-Aldrich	Cat#D6134; CAS: 154-17-6
Lipopolysaccharides from Escherichia coli O55:B5	Sigma-Aldrich	Cat#L6529
Fluorescein-5-Isothiocyanate	Thermo Fisher Scientific	Cat#F1906; CAS: 3326-32-7
MitoSOX Red	Thermo Fisher Scientific	Cat#M36008
MitoTEMPO	Sigma-Aldrich	Cat#SML0737; CAS: 1334850-99-5
MitoView Green	Biotium	Cat#70054
MitoTracker Red CMXRos	Thermo Fisher Scientific	Cat#M7512; CAS: 167095-09-2
4-Octyl itaconate	Sigma-Aldrich	Cat#SML2338; CAS: 3133-16-2
TRIzol	Thermo Fisher Scientific	Cat#15596026
PowerUp SYBR Green PCR Master Mix	Thermo Fisher Scientific	Cat#A25742
Mouse IL-10 Recombinant Protein	Thermo Fisher Scientific	Cat#RMIL105
Critical commercial assays		
GeneArt Precision gRNA Synthesis Kit	Thermo Fisher Scientific	Cat#A29377

(*Continued on next page*)

Continued

REAGENT or RESOURCE	SOURCE	IDENTIFIER
Succinate Colorimetric Assay Kit	Sigma-Aldrich	Cat#MAK184
Fumarate Assay Kit	Sigma-Aldrich	Cat#MAK060
Seahorse XFp Real-Time ATP Rate Assay Kit	Agilent Technologies	Cat# 103591-100
ABTS ELISA Buffer Kit	Peprotech	Cat#900-K00
Murine IL-1β Mini ABTS ELISA Development Kit	Peprotech	Cat#900-M47
Murine IL-6 Mini ABTS ELISA Development Kit	Peprotech	Cat#900-M50
Murine IL-10 Mini ABTS ELISA Development Kit	Peprotech	Cat#900-M53
Mouse IFN-β ELISA kit	Finetest	Cat#EM1148
Murine TNF-α Mini ABTS ELISA Development Kit	Peprotech	Cat#900-M54
Griess Reagent Kit for Nitrite Determination	Thermo Fisher Scientific	Cat#G7921
First Strand cDNA Synthesis Kit	Thermo Fisher Scientific	Cat#K1612
Experimental models: Cell lines		
RAW 264.7	ATCC	Cat#TIB-71; RRID:CVCL_0493
RAW 264.7 Sdha−/−	This paper	N/A
RAW 264.7 Sdhb−/−	This paper	N/A
HEK293FT cells	Thermo Fisher Scientific	Cat#R70007; RRID: CVCL_6911
Experimental models: Organisms/strains		
C57BL/6J	The Jackson Laboratory	Cat#000664; RRID:IMSR_JAX:000664
Oligonucleotides		
Oligonucleotides (see Table S2)	Sigma-Aldrich	https://www.sigmaaldrich.com/
Recombinant DNA		
pX330-U6-Chimeric_BB-CBh-hSpCas9	Cong et al., 2013	Addgene Plasmid #42230
pX330-Sdha	This paper	N/A
pX330-Sdhb	This paper	N/A
pBluescript II KS+	Stratagene	Cat#212207
pBLAST-Sdha	This paper	N/A
pBLAST-Sdhb	This paper	N/A
Software and algorithms		
CRISPOR	Concordet et al., 2018	http://crispor.tefor.net/
Wave version 2.6.3	Agilent Technologies	https://www.agilent.com/
Kaluza software version 1.1 Leica	Beckman Coulter Life Sciences	https://www.beckman.com/
ImageJ	Schneider et al., 2012	https://imagej.nih.gov/ij/
GraphPad Prism v.8.0	GraphPad Software	https://www.graphpad.com/
Other		
LightCycler 480 II, 96	Roche Diagnostics	Material #05015278001
Neon Transfection System	Thermo Fisher Scientific	Cat#MPK5000
Neon 100µl transfection kit	Thermo Fisher Scientific	Cat#MPK10096
Seahorse XFp Extracellular Flux Analyzer	Agilent Technologies	Model #S7802A
VersaMax microplate reader	Molecular Devices	https://www.moleculardevices.com/
Gallios Flow Cytometer	Beckman Coulter Life Sciences	https://www.beckman.com/

RESOURCE AVAILABILITY

Lead contact

Further information and requests for resources and reagents should be directed to and will be fulfilled by the lead contact, María Simarro msimarrogrande@gmail.com.

Materials availability

Sdha−/− and *Sdhb*−/− RAW 264.7 cells will be made available on request but may require payment for shipping/handling costs and a material transfer agreement if there is a potential for commercial application.

Data and code availability

Data reported in this paper will be shared by the lead contact upon request. This study does not report the development of any new code. Any additional information required to reanalyze the data in this paper will be made available from the lead contact upon request.

EXPERIMENTAL MODEL AND STUDY PARTICIPANT DETAILS

Cell lines

Sdha−/− and *Sdhb*−/− RAW 264.7 were generated using CRISPR/Cas9 tool as described in the STAR Methods Details section. HEK293FT cell line was used for lentiviral production.

Mice

This study was conducted with 6- to 8-week-old C57BL/6J mice of both sexes. The mice within each experiment were of the same age and sex. C57BL/6J mice were maintained under pathogen-free conditions and all procedures and experiments were carried out according to institutional guidelines for the Animal Care and Use Committee at University of Valladolid (Spain). Bone marrow-derived macrophages (BMDMs) were generated as previously described[6] with slight modifications. Briefly, mice were euthanized in a CO_2 chamber and death was confirmed by cervical dislocation. Bone marrow cells were extracted from leg bones and differentiated in DMEM (containing 10% fetal calf serum, 1% penicillin streptomycin and 10% L929 supernatant) for 8 days, at which time they were counted and replated for experiments. L929 culture supernatant was a gift from Dr. MA Balboa (Institute of Biomedicine and Molecular Genetics, Valladolid, Spain). When indicated, BMDMs were edited for *Sdha* and *Sdhb* as described in the Method Details section.

METHOD DETAILS

Plasmids construction

The targeting vectors were designed to delete *Sdha* and *Sdhb* using Cas9-induced homology-independent targeted integration (HITI) strategy.[15] gRNA sequences against the exon 1 of *Sdha* and *Sdhb* were designed using CRISPOR tool. Forward and reverse oligonucleotides containing the guide sequences for *Sdha* (CL1 and CL2) and *Sdhb* (CL3 and CL4) were annealed and cloned into the BbsI site of pX330-U6-Chimeric_BB-CBh-hSpCas9, generating two plasmids named pX330-Sdha and pX330-Sdhb, respectively. For the HITI donor plasmids production, forward and reverse primers were designed to contain the gRNA sequences for *Sdha* (CL5 and CL6) and *Sdhb* (CL7 and CL8), the PAM sequence, stop codons (CL5 and CL7) and 21–22 nucleotides corresponding to the 5′ (CL5 and CL7) and 3′ (CL6 and CL8) flanking regions of the floxed blasticidin cassete of the pBS-Blast plasmid. PCR products were cloned into BamHI and SalI sites of pBluescript II KS+. pBS-Blast plasmid was previously generated in our laboratory, and it is a pBluescript II based plasmid containing a blasticidin resistance cassette flanked by loxP sequences. The resultant donor plasmids were named pBLAST-Sdha and pBLAST-Sdhb. The sequences of the cloning primers CL1-8 are shown in Table S2.

Generation of *Sdha*−/− and *Sdhb*−/− macrophages

RAW 264.7 cells were transfected with pX330 plasmids (pX330-Sdha and pX330-Sdhb) and the corresponding HITI donor plasmids (pBLAST-Sdha and pBLAST-Sdhb) at a molar ratio of 3:1 and selected in medium containing 2 μ/ml blasticidin. Correctly targeted clones were identified by Sanger sequencing of PCR products. The PCR products showing double peaks were subjected to TA cloning and further sequenced. HITI-introduced mutations are provided in Table S1. The absence of Sdha and Sdhb proteins was confirmed by Western blotting.

Complex II activity

Complex II activity was assayed by electron transfer from succinate to the artificial electron acceptor 2,6-dichlorophenol-indophenol (DCPIP) via the coenzyme Q10 analog decylubiquinone as previously described with slight modifications.[16] The protonation of DCPIP by reduced decylubiquinone is reflected

by a decrease in absorbance at 600 nm The intracellular succinate (SDH substrate) and fumarate (SDH product) concentrations were measured with colorimetric and UPLC-MS assays.

Seahorse metabolic analysis

Oxygen consumption rate (OCR) and extra cellular acidification rate (ECAR) were assessed in the extracellular analyzer XFp. Mitochondrial respiration assays were performed following the described protocol[53] with minor modifications in reagents concentrations: 2.6 μM oligomycin, 1 μM carbonyl cyanide 4-(trifluoromethoxy) phenyl-hydrazone (FCCP) and 1 μM rotenone/antimycin A. ATP production from glycolysis and mitochondria was measured using the Seahorse XFp Real-Time ATP rate assay Kit. 40.000 cells/well were seeded for approximately 24 hours on XFp plates prior to performing the tests. In some experiments, the cells were preincubated with 200 ng/mL Lipopolysaccharides (LPS) from *Escherichia coli* 055:B5 for 4 hours prior to the assays. Data was obtained using Agilent Seahorse Wave 2.6.3 software.

Measurement of cytokines and nitric oxide (NO)

IL-1β, IL-6, IL-10 and TNF-α levels were measured using ELISA kits. The determination of nitrite as a marker of NO production was performed through the Griess reaction method. In all cases, manufacturer's instructions were followed. Absorbances were measured on a VersaMax microplate reader. Macrophages were stimulated with 100 ng/ml LPS, and cells were collected at 4 hours for cytokines mRNA quantification by real-time PCR, supernatants were collected at 8 hours for cytokines measurements by ELISA, and at 24 hours for nitrite determinations. In all the experiments, macrophages ($3x10^5$) were seeded in 24 well plate for approximately 24 hours prior to LPS stimulation. The culture media was replaced with phenol red-free media before the addition of LPS when the supernatants were to be analyzed with the Griess reagent. When indicated, cells were preincubated in the presence of SDH inhibitor DMM (16 mM) for 1 h or 7 days prior to the addition of LPS.

Phagocytosis and bacterial killing assays

Phagocytosis of fluorescently labeled bacteria was measured by flow cytometry. Heat-killed *Escherichia coli* (80°C, 15 min) were incubated with a 0.1 mg/ml solution of Fluorescein-5-isothiocyanate (FITC) at 37°C for 30 min and washed three times with PBS prior to use. FITC-labeled bacteria were added to $5x10^5$ macrophages at a 100:1 ratio for 30 min at 37°C. Macrophages were then washed three times with cold PBS, and extracellular FITC-labeled bacteria were quenched with a 60 s wash in trypan blue (0.2 mg/ml). Macrophages were fixed with 4% paraformaldehyde and analyzed by flow cytometry using a Beckman Coulter Gallios. Where indicated, cells were pretreated with Compound C: AMPK inhibitor (10 μM, 30 min) prior to phagocytosis assays. The bactericidal activity was studied using gentamicin protection assay. Briefly, $5x10^5$ cells were infected with *Escherichia coli* with a multiplicity of infection (MOI) of 100. After 15 min of incubation at 37°C, the nonadherent extracellular bacteria were removed by washing with PBS, and the adherent extracellular bacteria were subsequently killed by the addition of medium containing gentamicin (100 μg/ml) for an additional 15 min. At time 0 h (which corresponds to the end of the gentamicin treatment) and time 2 h, cells were washed three times with PBS and lysed with 1 ml of sterile distilled water. Serial dilutions of cellular lysates were plated onto Luria–Bertani agar plates, and the number of CFUs was determined after 24-h growth at 37°C. The percentage of killed bacteria was calculated as follows: % killing = 100 - [(no. of CFU at time 2 h/no. of CFU at time 0 h) x 100]. The bacterial strain used in these assays was *Escherichia coli* DH5a.

Flow cytometry

MitoTracker Green (for total mitochondrial mass), MitoTracker Red CMXRos (for mitochondrial membrane potential) and MitoSOX (for mitochondrial ROS) staining were performed according to manufacturer's instructions. Intracellular iNOS staining was performed with mouse monoclonal CXNFT labeled to APC according to manufacturer's instructions. For flow cytometry analysis, data were acquired with a Gallios Flow Cytometer and analyzed with Kaluza version 1.1.

Real-time PCR

Total RNA was extracted using TRIzol reagent. RNA (1 μg) was reverse transcribed using First Strand cDNA Synthesis Kit to generate cDNA that was quantified by real-time PCR analysis with the LightCycler 480 Instrument using PowerUp SYBR Green PCR Master Mix. Primers pairs were designed for amplification of Arg1 (RT1/RT2), Bcl3 (RT3/RT4), Hprt (RT5/RT6), IFN-β (RT7/RT8), IL-10 (RT9/RT10), and Socs3 (RT11/RT12). Primer

sequences are provided in Table S2. Relative mRNA expression was obtained using the ΔΔCt method using Hprt as reference gene.

Western blotting

Protein was extracted by RIPA buffer plus protease inhibitors. Twenty-microgram protein samples separated by SDS-PAGE and transferred to PVDF membranes. The membranes were used for the immunodetection of β-actin, AMPKα, AMPKα pT172, HIF-1α, Sdha, Sdhb, Stat3, Stat3 pY705, and Stat3 pS727. Band intensities were determined by densitometric analysis using ImageJ software. In all the experiments, macrophages ($3x10^5$) were seeded in 24 well plate for approximately 24 hours prior to stimulation with LPS (100 ng/ml) ~~or~~,LPS + IL-10 (1–10 ng/ml), LPS + DMM (16 mM or 32 mM), LPS + DMF (25 μM), LPS + OI (125 μM), or LPS + mitoTEMPO (50 μM or 100 μM).

Extraction and assay of metabolites

RAW 264.7 cells were left untreated or treated with 100 ng/ml LPS for 24 h, and then the extraction and assay of metabolites were performed as previously described.[55] Cells were treated with cold acetonitrile/methanol/water (2:2:1, v/v/v), frozen in cold nitrogen, and thawed prior to bath sonication for 15 min at 4°C. After an additional cycle of freezing and sonication, the extracting mixture was kept at −20°C for 1 h and then centrifuged at 15,000 xg at 4°C for 15 min for deproteinization. The supernatant was recovered and evaporated to dryness.[56] The dry extract was solubilized in acetonitrile/water (1:1, v/v), sonicated, and centrifuged to remove insoluble material. The sample solvent was evaporated to dryness and the pellet resuspended in Milli-Q water. The assay of intracellular lactate, citrate, itaconate, succinate, malate, and oxaloacetate were done using an UPLC-MS assay. The chromatographic separation was carried out with an Acquity CORTECS UPLC C18 column (Waters) directly interfaced into the electrospray ionization source of a Q-TOF mass spectrometer (SYNAPT HDMS G2, Waters). An elution gradient involving the eluents (A) H2O/methanol/formic acid (95:5:0.1, v/v/v) with 5 mM ammonium formate, and (B) 100% acetonitrile with 0.1% formic acid and 5 mM ammonium formate, was run from 95% A to 20% A in 4 min, then isocratic until 4.5 min, to come again to 95% A at 6 min and kept to 95% A for an additional period of 2 min (8-min elution period), at a flow rate of 0.2 ml/min. MS analysis was performed in the negative ion mode using an MSE method that allows simultaneous detection of analytes through a low-energy function (full scan) and a high-energy function (collision energy) with ion partial fragmentation. All of the metabolites were detected as the [M-H]− ion except oxaloacetate, which was detected as the [M-H2O-H]− ion.

QUANTIFICATION AND STATISTICAL ANALYSIS

Statistical analyses were performed using GraphPad Prism software. Data were analyzed by ANOVA followed by Tukey's multiple comparison test or by unpaired, two-tailed t test. Values of $p < 0.05$ were considered statistically significant. In the figures, each point represents a biological replicate and, if no other indication is made, data are expressed as the mean ± SEM.

ADDITIONAL RESOURCES

Not applicable.